

Modelling the morphodynamic impact and the effect on significant wave height due to sand extractions.

A model study for the Holland coast area.

Final thesis

B. Fakkert



UNIVERSITY OF TWENTE.

To be presented at the University of Twente on Friday 8 January 2016

Date 30 Dec 2015

Version Final

Author Benno Fakkert

Contact benno.fakkert@gmail.com

University University of Twente

Faculty Engineering Technology (ET)

Program Water Engineering and Management (WEM)

Graduation Prof. dr. S.J.M.H. Hulscher (chair)

committee Dr. ir. B.W. Borsje (daily supervisor)

Dr. ir. P.C. Roos (daily supervisor)

R. Hoogland, MSc

University of Twente

University of Twente / Deltares

University of Twente

Rijkswaterstaat Water Verkeer en

Leefomgeving

Abstract

This thesis presents a study into both the morphodynamic effects as well as the hydrodynamic effects in terms of the significant wave height of a sand extraction in the coastal area of the Holland coast. Due to the reduction of available sand and possible cost reductions, Rijkswaterstaat is interested in the effects of new sand extractions strategies on the safety of the coast, i.e. larger extractions in terms of depth as well as extractions closer to the shore in the Holland coast part of the Dutch coast than current regulation allows.

For the morphodynamic impact of a sand extraction also referred to as a sand pit, we built a process-based idealized sand pit model (referred to as the 2015 sand pit model), based on a previous sand pit model (referred to as the 2008 sand pit model). The 2015 sand pit model is used for flow, sediment transport and bed evolution in a tide-dominated environment. The 2015 sand pit model will enable a multi-directional basic flow, where the 2008 sand pit model used a unidirectional basic flow. The multi-directional flow is a more realistic representation of the tidal flow and allows for tidal ellipses with arbitrary orientation, amplitude, and eccentricity. Tidal current data is gathered from the MATROOS model of Rijkswaterstaat and a harmonic analysis is performed with the MatLab program `t_tide` to reproduce a realistic tidal signal.

For the impact of a sand pit on the significant wave height we use the Delft3D-WAVE model with storm conditions corresponding to recurrence times of 100, 1,000, and 10,000 year in the Holland coast. These storm conditions are water level, significant wave height, peak period, wind speed, wind direction, and wave direction. The Delft3D-WAVE model is used to simulate the evolution of wind-generated waves in coastal waters. The model computes wave propagation, non-linear wave-wave interactions and wave dissipation, for a given bottom topography and water level. We choose to omit the morphodynamic effects during storm conditions and only look at the change in significant wave height. Multiple bed profiles are gathered from bathymetry data of the Holland coast and are used to make a schematized two-dimensional bed profile. A sensitivity analysis for both models is carried out to analyse the effects of pit geometry and position on the model results.

The morphodynamic effects in the 2015 sand pit model are presented in terms of area of morphodynamic influence, pit deepening, radius of morphodynamic influence and migration. The morphodynamic effects after 50 years are found to be small. Furthermore, the 2015 sand pit model results show that sand pits trigger the morphodynamic instability associated with the formation of large-scale bed features known as tidal sandbanks. A gradual deformation of the pit itself can be observed, as well as the appearance of adjacent humps. The corresponding time scale is of the order of decades to centuries, where the time-scale decreases for pits at smaller water depths. Finally the migration rate is independent of the pit geometry and depends only on the tidal flow conditions, this agrees with previous findings.

The change in significant wave height in the Delft3D-WAVE model is found to be stronger for deeper pits and pits closer to the shore with the used model settings. A decrease in significant wave height is found landward of the pit due to diffraction. Areas with an increase in significant wave height are found locally next to pit. The increase in significant wave height in the BCL zone is negligible and in the rest of the coastal foundation the relative increase is in the order of a few percent.

It can be concluded with the used models and underlying assumptions that both large scale sand extractions at the 20 m NAP depth line and small scale sand extractions closer to the shore

result in relatively small changes with respect to the situation without a sandpit. It has to be mentioned that the 2015 sand pit model predicts tidal sand banks whereas in the study area shoreface connected ridges are present with a different orientation. It would be recommended to add wind driven sediment transport, which enables for the growth of shoreface connected ridges.

Preface

This report presents the final project of my study Water Engineering and Management at the University of Twente. I had a great time living in Enschede and made a lot of friends. I want to thank you all for making my time in Enschede extra special. A special thanks for my fellow students from my graduation room at the university of Twente for the great time. I also would like to thank the inspiring and enthusiastic teachers who made me enjoy this study even more. I also would like to thank the teachers for making it possible to follow video lectures while I visited Argentina and Uruguay for the international study tour Latin Links.

This thesis will hopefully play a role in future coastal management decisions. The last few months I have had the opportunity to work on my final thesis at Deltares in Utrecht. I would like to thank my colleagues there for the great time and would especially like to thank my supervisors Laura Vonhögen-Peeters from Deltares and Rena Hoogland from Rijkswaterstaat for the supervision, the useful input and their feedback on my thesis.

In the beginning of my thesis I spent a lot of time at the University of Twente for the model development and would like to thank my supervisor Pieter Roos for his assistance with the model. I really enjoyed programming the MatLab model. Furthermore I would like to thank my other supervisor Bas Borsje for his input and creative ideas during my thesis and as last I would like to thank the head of my examination committee Suzanne Hulscher for her questions and feedback on my thesis.

Last but not least I would like to thank my family, friends and girlfriend for the great support.

I worked with great pleasure on the subject and learned a lot, thank you all!

Benno Fakkert
Utrecht, December 2015

Contents

1	Introduction	8
1.1	Problem definition	11
1.2	Research goal and questions	13
1.3	Methodology	13
2	Holland Coast area	16
3	Sand pit model	23
3.1	Model geometry	23
3.2	Model equations	23
3.3	Scaling procedure	24
3.4	Basic flow conditions	24
3.5	Solution method	25
3.6	Indicators	26
4	Delft3D-WAVE model	27
4.1	Model schematization	28
4.2	Model runs	29
4.3	Indicator	30
5	Results	31
5.1	2015 Sand pit model	31
5.2	Delft3D-WAVE model	39
5.2.1	Different pit locations	40
5.2.2	Different pit depths	42
5.2.3	Different angle of incidence	44
6	Discussion	47
7	Conclusions and Recommendations	48
7.1	Conclusions	48
7.2	Recommendations	49
8	References	50
9	Appendix	52
9.1	Future sand extraction scenarios	52
9.2	Tidal current data	53
9.3	Scatter plots of x- and y- velocities	54
9.4	Dike ring area 14	55
9.5	Scaling procedure	56
9.5.1	Sediment transport	57
9.5.1	Bed evolution	57

9.6	Solution method	58
9.7	Linearizing the equations with respect to the bed amplitude.	59

1 Introduction

This study is part of the coastline care project “KPP BenO kust” which is performed in collaboration between Rijkswaterstaat WVL (ministry of Infrastructure and the Environment) and Deltares.

Large parts of the Netherlands are prone to flooding as a result of the many rivers and because of the many areas below sea level. Therefore protection of the hinterland is of great value. The Dutch coastal policy strives to use soft protection measures for the coastal protection whenever possible (Elias & Bruens, 2013). Most of the Dutch coast consists of sandy beaches and dunes. Due to erosion, sand nourishments have to be performed in order to maintain the coast. The sand needed for these nourishments is obtained from sand extractions in the Dutch part of the North sea. The pit that is left behind after the extraction is finished is referred to as a sand pit.

Coastal policy

In order to stop structural recession of the coastline, the Dutch government specified a clear operational objective: *the coastline will be maintained at its position in the year 1990.*

In order to assess the condition of the system the concept of the Momentary Coastline (MCL) has been developed, defining the coastline position as a function of the volume of sand in the near shore zone. The calculation of the MCL is based on volume per unit length of sand between two horizontal planes. The upper and lower boundaries are located at a distance ‘H’ from the mean low water level, where ‘H’ denotes the vertical difference between the dune foot and the mean low water level (see Fig. 1) (van Koningsveld and Mulder, 2004). The position of the upper and lower planes are approximately +3 m NAP and 5 m NAP respectively (Giardino et al., 2012) (NAP, Normaal Amsterdams Peil is Dutch Ordnance Level approximately equal to Mean Sea Level (Van Koningsveld and Mulder ,2004))

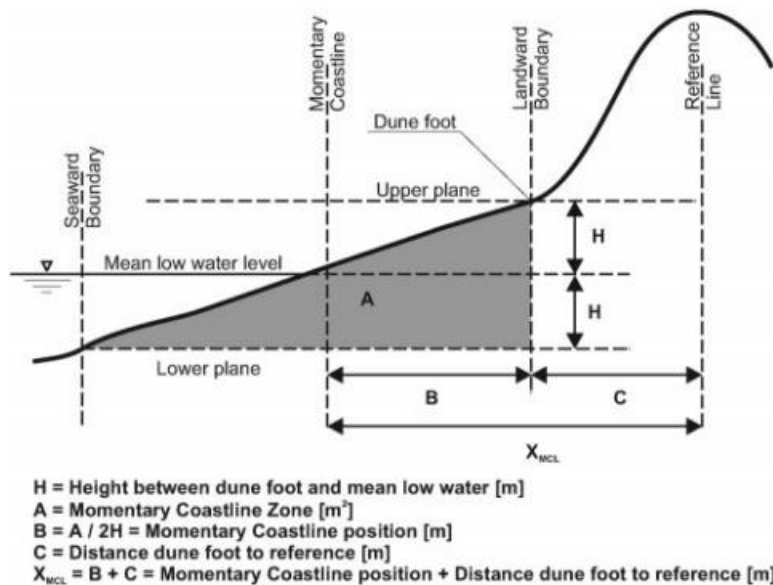


Figure 1 Calculation of Momentary Coastline (MCL) (Source: Van Koningsveld and Mulder, 2004)

The Basal Coastline (BCL) has been defined as the estimated position of the coastline on January 1st of 1990. The description of the actual state of the system is based on a so-called Testing Coastline (TCL). The position of the TCL is determined by linearly extrapolating the trend of the coastline positions (MCL) of ten previous years. The state of the system can now be compared with the reference state, by comparing the TCL position with the BCL position. This comparison provides an indication for the expected coastal state in a year. A TCL that

moves landward of the BCL represents a signal for coastal management to consider intervention. (Van Koningsveld and Mulder, 2004)

The policy of the maintenance of the coastline alone is not sufficient. This policy does not consider the morphological development at larger scale, induced for example by sand losses at larger water depth and by sea level rise. The hypothesis is that sand losses at larger water depth could, in the long term, lead to a loss of sediments also in the upper shoreface. This would result in an extra future afford for maintaining the coastline. An extra concept is developed: The compensation of loss of sediments due to sea level rise including the whole Coastal Foundation. The Coastal foundation is defined as the area between the inner edge of the dune and the established -20 m NAP depth line, see Fig. 2 (Giardino et al., 2012).

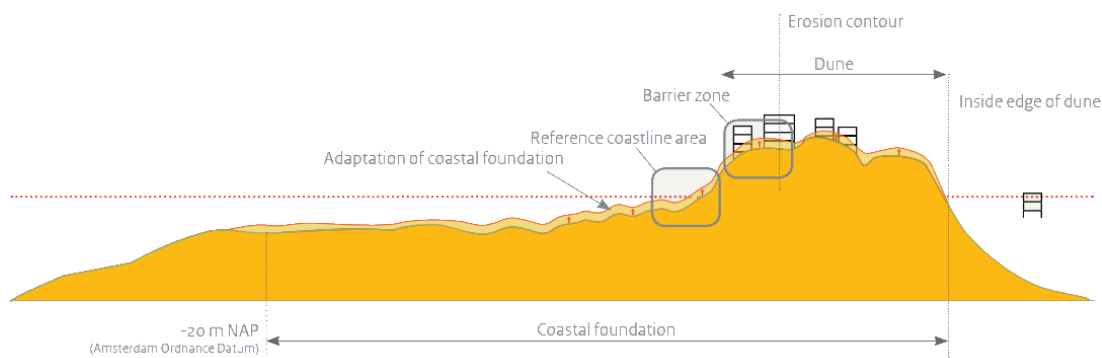


Figure 2 The coastal foundation covers the zone from the established -20 m NAP depth line at sea up to and including the inside edge of the dune. (Source:(Delta Programme), n.d.)

The Dutch coastal management establishes a nourishment scheme in order to maintain the coastline and the coastal foundation. The total nourishment volume carried out for regular maintenance of the coast for the period 2004-2014 can be found in Fig. 3

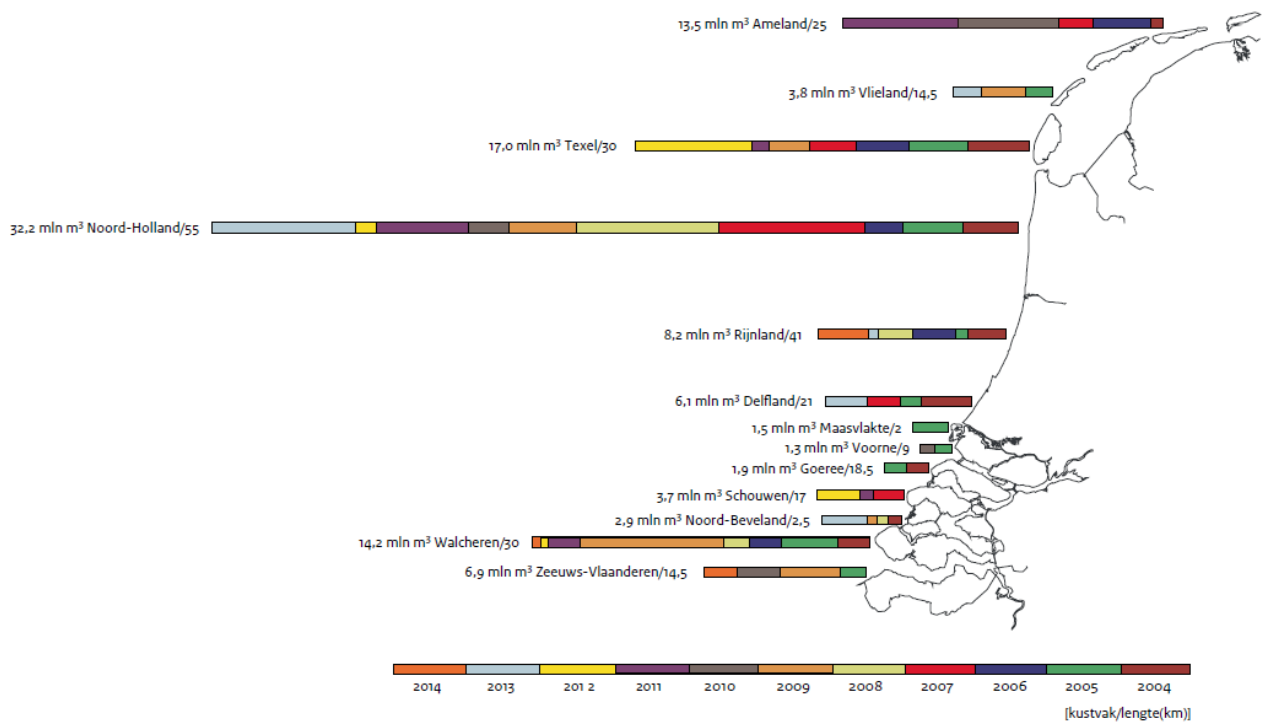


Figure 3 Total Nourishment volume per coastal section carried out for regular maintenance of the coast for the period 2004-2014 (Source:(Rijkswaterstaat, 2014))

Extraction regulations

Current regulations concerning sand extractions are the following (Ministerie van Verkeer en Waterstaat, 2004):

- Only extractions seaward of the established 20 m NAP depth line are allowed.
- The minimum distance from an extraction pit to off-shore infrastructure is 500 m.
- A distinction is made between small-scale extraction (< 10 million m³) and large-scale extraction (> 10 million m³)
- For a large-scale extraction or an extraction covering an area larger than 500 hectares, an Environmental Impact Assessment (EIA) is required. This also applies to multiple small scale extractions close to each other.
- Pit depths up to 2 m are allowed. For large-scale extractions, it is possible to extract deeper than 2 m if an EIA shows that this is acceptable.
- Furthermore an extra seaward shift of 2 km is added to the established -20 m NAP depth line as restriction for large-scale extractions, to allow sufficient space for small-scale extractions can be executed close to the shore.

1.1 Problem definition

For cost effectiveness, sand extractions are preferably performed close to the nourishments, in this way dredging ships travel relatively short distances and therefore reduce the fuel costs. By changing the topography of the seabed the hydrodynamics and the morphodynamics also change. Because topography changes may affect the safety of the coast, by means of disturbing the sediment balance in the coastal foundation, sand extractions are currently only allowed seaward of established 20 m NAP depth line. In 1991 it was determined that extractions landward of the physical 20 m NAP depth contour are not allowed (Ministerie van Verkeer en Waterstaat, 1991). Because the physical 20 m depth contour is subject to change, the so-called established 20 m NAP depth line was introduced in 2004 (Ministerie van Verkeer en Waterstaat, 2004). The laws of the Dutch government apply until 12 nautical miles offshore. This results in a reserved area for sand extractions, as shown in Fig. 4.

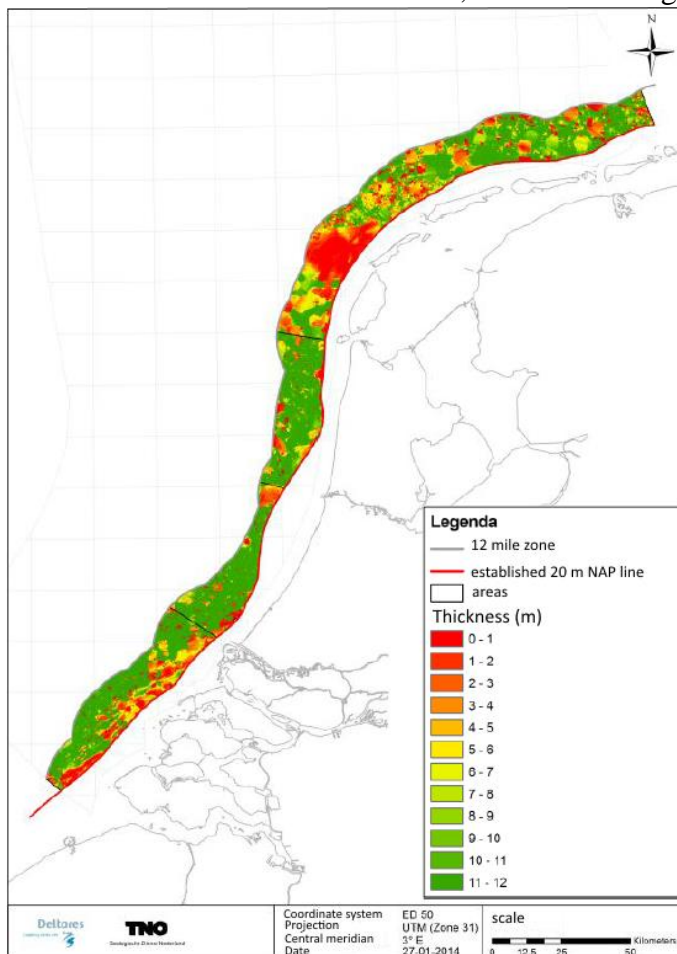


Figure 4 Reserved dredging area between the 12 nautical mile zone and the established 20 m NAP line. The colors represent the thickness in meter of the available sand layer. (Source: Maljers-Oosterwijk et al. (2014))

As can be seen in Fig. 4, a seaward shift of the established 20 m NAP depth line is present in front of the Holland Coast (See Fig. 5 for the definition of the Holland Coast). This results in a smaller reserved area for sand extractions and a larger shipping distance for dredging ships than areas where the established 20 m NAP depth line is positioned closer to the shore.

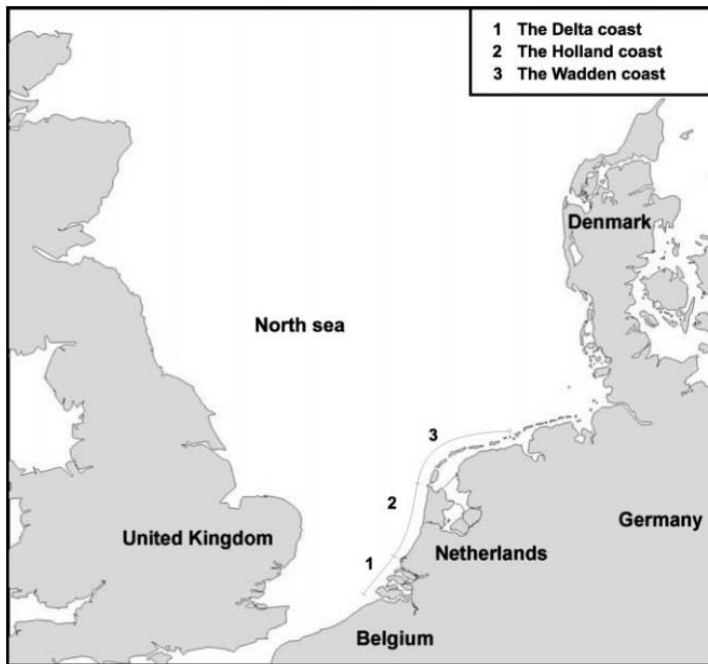


Figure 5 Orientation on the coast of Netherlands and its three sub-regions (Source: Van Koningsveld and Mulder (2004))

The annual sand extraction volume in the Netherlands increased in the past decades due to new coastal safety approaches. Currently the average annual nourishment volume is 12 million m³ (Elias & Bruens, 2013), different scenarios describe an increase in the annual extraction volume between 25 and 110 million m³ (where 13 to 25 million m³ is for commercial use) up to the year 2100 (see appendix 9.1) (Vonhögen-Peeters et al., 2012).

Therefore, especially in front of the Holland Coast, problems could arise because the reserved dredging area may not provide enough sand in the future to meet the annual extraction volume. Because of this Rijkswaterstaat want to explore new sand extraction strategies. These strategies are as follows:

- Perform large scale sand extractions directly at the established -20 m NAP depth line.
- Perform small-scale extractions landward of the established -20 m NAP depth line.

1.2 Research goal and questions

The research goal is threefold and is stated as follows:

- i. *To determine the effects of a large-scale sand extractions within the 2 km zone seaward of the established 20 m NAP depth contour in front of the Holland Coast, and*
- ii. *to determine the effects of a small-scale sand extractions landward of the established 20 m NAP depth contour in front of the Holland Coast.*
- iii. *(As an additional goal of the thesis) to make a deliverable MatLab sand pit model, with a multidirectional flow input, for Rijkswaterstaat and Deltares. In order to do this we will use the sand pit model of Roos et al (2008), which uses a unidirectional flow.*

Based on the problem definition and the research goal, the following main research questions are to be answered.

1. What is the effect of a large scale extraction within the 2 km zone seaward of the established 20 m NAP depth line in front of the Holland Coast?
2. What is the effect of sand extractions landward of the established -20 m NAP depth line in front of the Holland Coast?

To answer these main research questions, the following sub-questions are to be answered.

1. What is the minimal increase in area of morphodynamic influence?
2. What is the minimal pit deepening value?
3. What is the minimal radius of morphodynamic influence?
4. What is the value for migration of the pit's centre of 'mass'?
5. What are the effects of a deeper sand pit in terms of morphodynamic influence?
6. What are the effects of a deeper sand pit in terms of significant wave height?

1.3 Methodology

This research assesses the effects of the new sand extraction strategies by means of determining the tidal driven morphological evolution of a sand pit in time (keeping offshore tide-dominated conditions in mind, the effects of wind waves on hydrodynamics and sediment transport are neglected) as well as determining the effects of a sand pit on the significant wave height, which can be used as an indicator for erosion, under storm conditions. We choose to investigate the effects in terms of significant wave height, because in shallow water and during storm conditions (which take place on relatively small time scales) the effect of wind waves on sediment transport is large. This approach gives Rijkswaterstaat an indication of the effects the new sand extraction strategies might have on the safety of the coast.

In this research we need to use two models, because the effects we are interested in cannot be calculated with one model. First, we will develop a process based semi-analytical sand pit model to describe the tidal driven morphological evolution of a sand pit. Secondly, we will use the process based numerical Delft3D-WAVE model to assess the change in significant wave height under storm conditions due to the geometry of a sand pit.

The sand pit model we will develop is based on the sand pit model of Roos et al. (2008), which will be referred to as the 2008 sand pit model from now on. This results in a semi-analytical tool that, unlike previous studies, enables a quick and extensive study into the effects of varying the physical characteristics as well as the pit design parameters. These parameters include pit length, width, and orientation.

2015 sand pit model

The 2008 sand pit model is written in the programming language Fortran, for practical use we write the new sand pit model in the programming language MatLab. Furthermore, the 2008 sand pit model uses a unidirectional tidal flow as input, so we develop a new sand pit model (from now on referred to as 2015 sand pit model) which uses a multidirectional tidal flow as input which allows for tidal ellipses with arbitrary orientation, amplitudes and eccentricity.

For the development of the 2015 sand pit model, we use the depth averaged shallow water equations to describe the hydrodynamics. Furthermore, we use a sediment transport equation and a bed evolution equation to describe the morphodynamics. We will scale the equations with dimensionless quantities and we will also apply a linearization with respect to the bed amplitude.

To get realistic tidal flow input for the 2015 sand pit model, we will use the MATROOS model from Rijkswaterstaat to get current data on a location in front of the Holland coast. Since the tidal flow does not vary that much locally, we have chosen an arbitrary location landward of the established 20 m NAP depth line in front of the Holland coast. With the MatLab program `t_tide` a harmonic analysis is performed on the current data to get the parameter values which can be used to describe a tidal ellipse. The input data is referred to as basic flow.

The basic state of the 2015 sand pit model describes a spatially uniform tide over a flat bottom where the flow vector is represented as a tidal ellipse. A perturbed state is obtained after implementing a sand pit. To solve for the perturbed flow an expansion is made into a discrete Fourier series. Per mode the evolution can be calculated and by using an inverse Fourier transformation the actual topography at any given point in time can be calculated.

We will perform a sensitivity analysis with the 2015 sand pit model for different pit geometries (basic state water depth, pit depth, length to width ratio, and orientation of the pit). In order to perform a sensitivity analysis we introduce four indicators: The area of morphodynamic influence, the radius of morphodynamic influence, pit deepening, and migration.

The area of morphodynamic influence is defined as the area where the difference between the actual topography and the undisturbed seabed exceeds a certain fraction of the pit depth. The radius of morphodynamic influence is defined as the radius of a circle enclosing the disturbed area of morphodynamic influence. Pit deepening is defined as the ratio between the initial pit depth and the pit depth after morphodynamic evolution at a certain point in time. Migration is defined as the motion of the pit shape's centre of 'mass'.

Delft3D-WAVE model

First we will make a 2D schematization of the Holland coast based on the average slope of the seabed profile in cross-shore direction. We assume the 2D schematization to be uniform in longshore direction.

For the boundary conditions of the Delft3D-WAVE model we impose conditions corresponding to storms with various recurrence intervals. These conditions are: water

level, significant wave height, peak period wave direction, wind speed, and wind direction. We can now gather the distribution of the significant wave height over the 2D schematization. This distribution will serve as the reference situation.

Next we will implement a sand pit to determine the effects of the sand pit on the significant wave height compared to the reference situation. We will vary in pit location and pit depth.

For a quantitative comparison we will determine the maximum increase in significant wave height for different storm scenarios in the BCL zone (-5 m NAP to +3 m NAP) as well as the rest of the coastal foundation (established -20 m NAP depth line to -5 m NAP). This increase in significant wave height is presented in a relative and absolute change (the results are relative to the reference situation with the same recurrence period).

2 Holland Coast area

This study focuses on the coastal area in front of the Holland coast (See Fig. 5). This area is located in the Dutch Continental Shelf, which is part of the North Sea. The seaward shift of the 20 m NAP depth line (the seaward boundary of the coastal foundation) can be seen in Fig. 6. Due to this shift sand extractions must be performed further offshore compared to other coastal areas, this is why we focus on this area in the study.

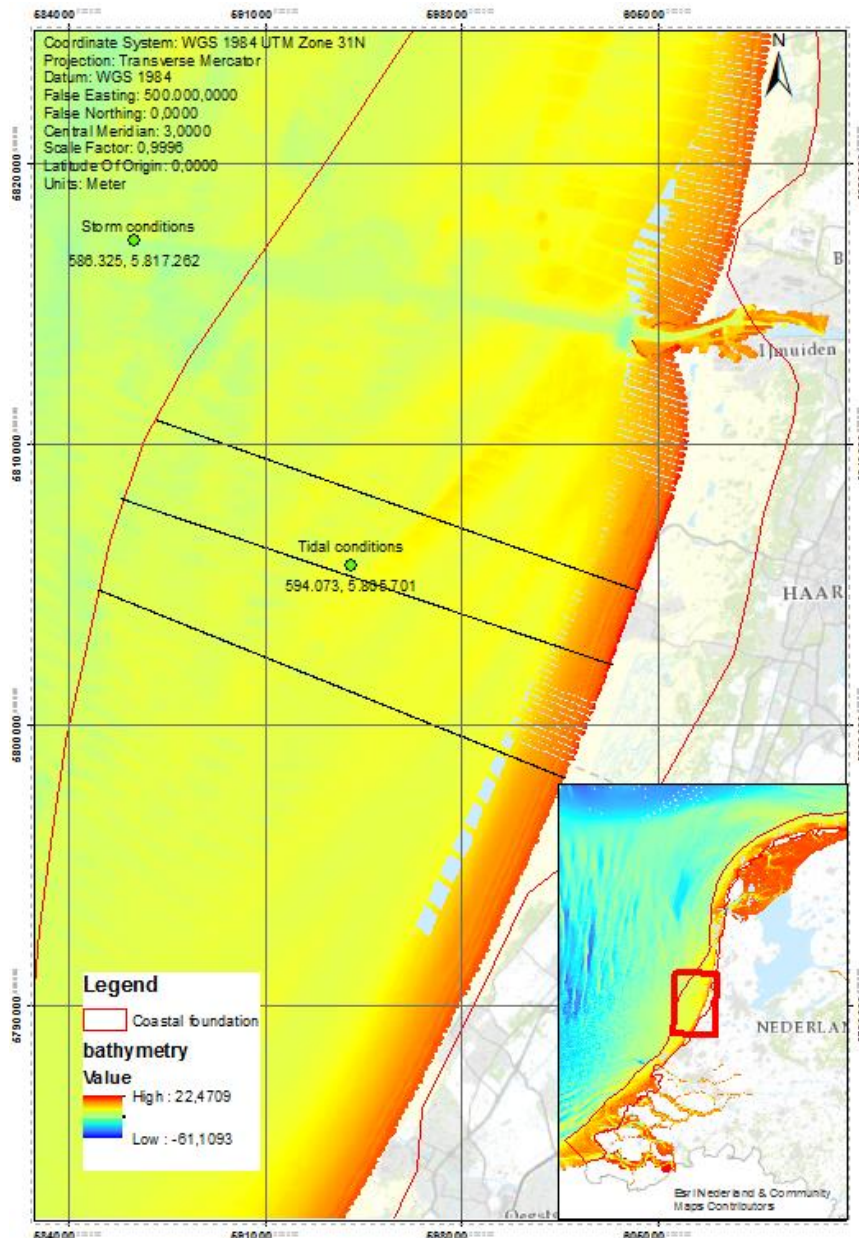


Figure 6 Study area, with: the tidal conditions location, the storm conditions location, 3 locations (black lines) for the depth profiles. (Bathymetry data: Royal Dutch Navy)

Bed level

A distinct transition in the slope of the seabed around -15 m NAP can be found between the red and yellow areas in Fig. 6. This transition in the bed slope can also be seen in Fig. 7, which shows the depth profiles from the three locations in Fig. 6. These bed slopes are used in the Delft3D-WAVE model for the schematization of the seabed.

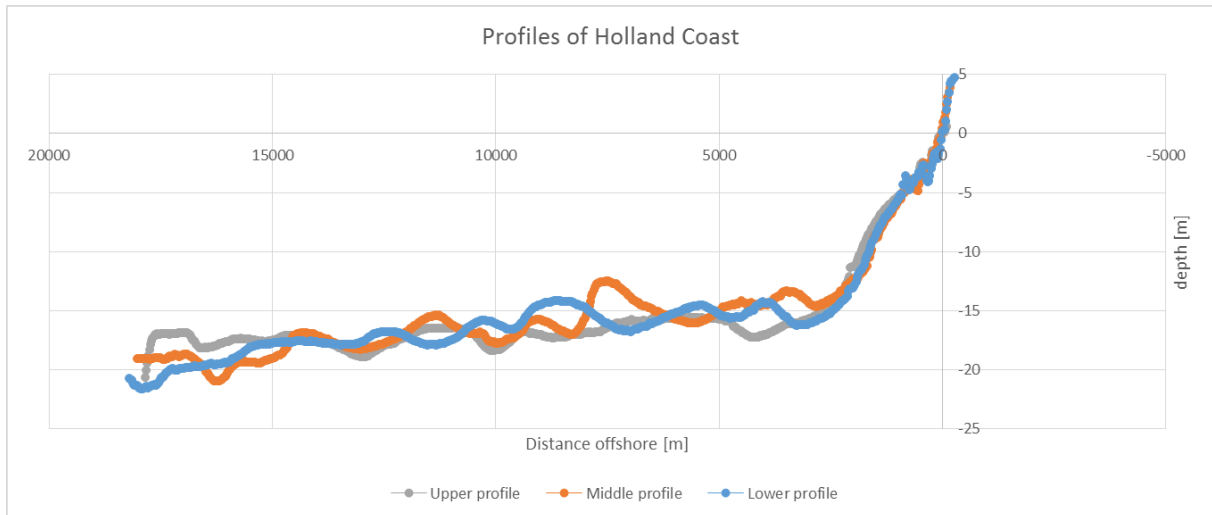


Figure 7 Depth profiles of the Holland coast.

Morphodynamic features

The seabed of the Dutch Continental Shelf consists mostly of sand. In this seabed a variety of rhythmic features is present. The characteristics of these features are given in table 1

Table 1 Characteristics of morphodynamic bed features (Dorst, 2009).

	wavelength	max. height	migration rate
Ripples	~1 m	0.01 m	~1 m/hour
Mega ripples	~10 m	0.1 m	~1 m/day
Sand waves	~500 m	5 m	~10 m/year
Sand banks	~6 km	10 m	~1 m/year

It can be seen that for large bed forms, the migration rate is very low. Since the sand pit can be seen as a large inverted bed form, migration rates of the sand pit are expected to be low (order 1-10 m/year) (Roos and Hulscher, 2003).

The 2015 sand pit model considers a flat sea bed, but in Fig. 8, which shows the distribution of bed features in front of the Dutch coast, it can be seen that this is not the case. This has to be taken into account when analysing the results.

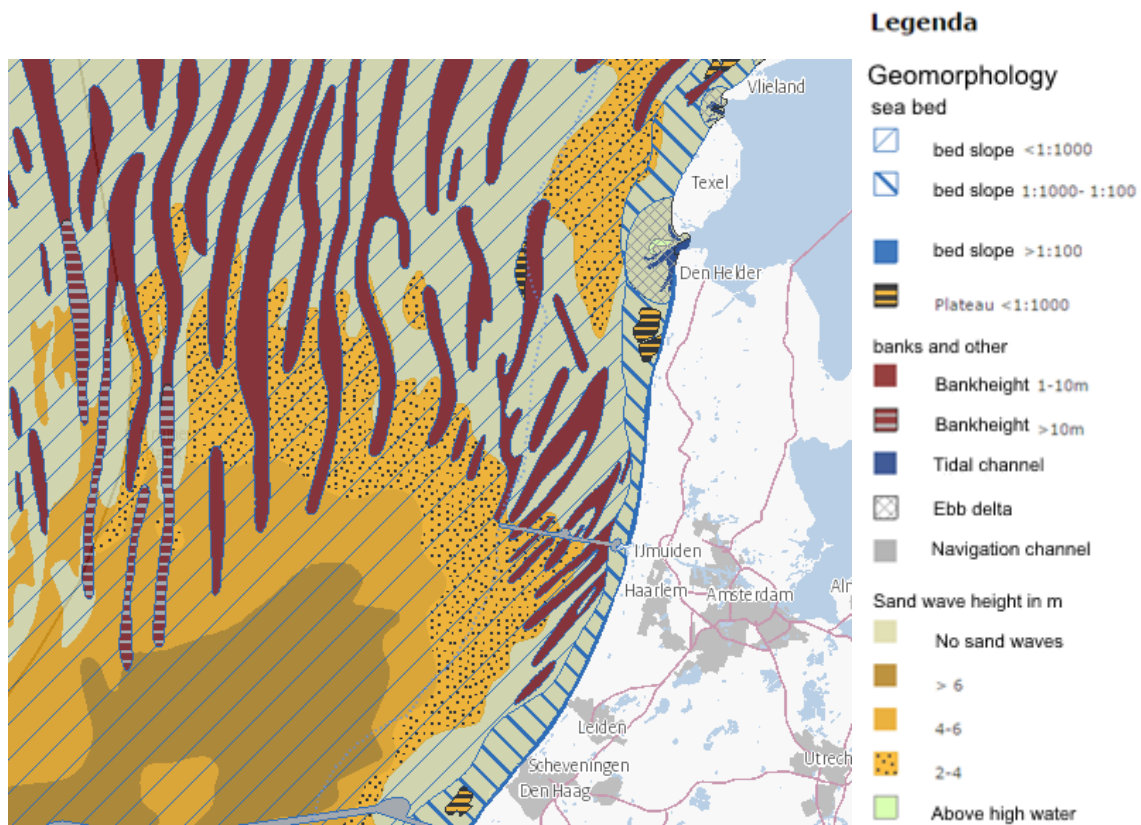


Figure 8 Schematized overview of the seabed in front of the Dutch coast. With sandbanks in red and sand waves of different heights in brown/orange("Geomorfologie NCP," n.d.) .

Sediment

The sediment grain size is inversely related to the amount of sediment transport (for non-cohesive sediments), in general a smaller grain size results in a larger sediment transport. Although the 2015 sand pit model does not take the grain size into account, it is valuable to see whether there is a large variation in grain sizes. The distribution of the grain sizes can be seen in figure 4. It can be seen that the seabed in front of the Dutch coast mostly consists of medium sand (250-500 μm), with finer sand (125-250 μm) close to the shore.

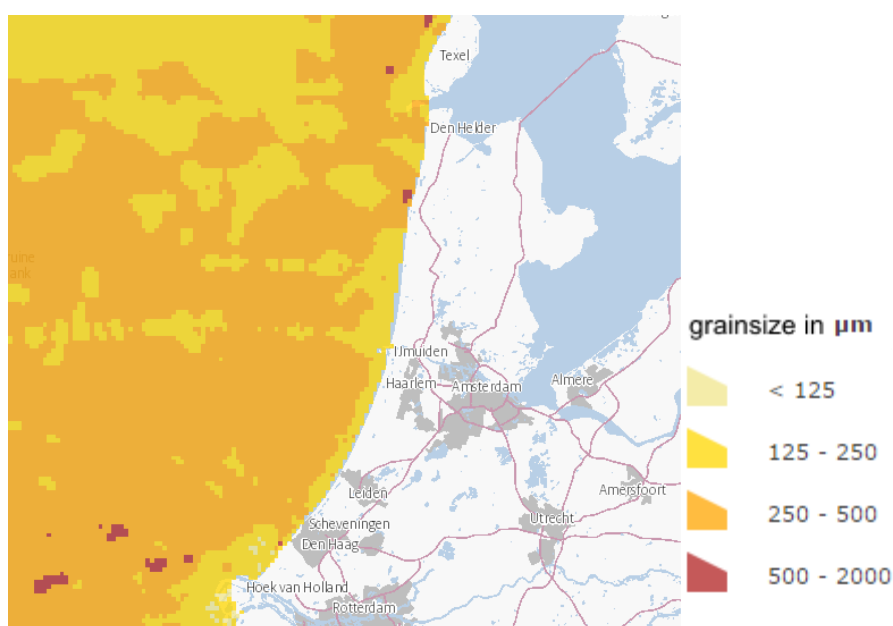


Figure 9 Grain size distribution over the seabed in front of the Dutch coast ("Korrelgrootte zand," n.d.).

Tidal conditions

Tidal data is used as input for the 2015 sand pit model, this information is gathered at the location given in Fig. 6 using the online MATROOS model from Rijkswaterstaat. From the MATROOS model tidal data is obtained in the form of a velocity in x- and y-direction (east and north respectively). This velocity data is transformed into tidal components using a harmonic analysis. This harmonic analysis is done with the MatLab program T_Tide as described in Pawlowicz et al. (2002). The result of the harmonic analysis is a series of tidal components where each component is composed of the following parameters:

- Semi-major (SEMA), the maximum current velocity, which is the length of the main axis of the tidal ellipse.
- Semi-minor (SEMI), the minimum current velocity, which is the length of the axis perpendicular to the semi-major axis.
- Phase, the phase lag of the tide with respect to the maximum current velocity.
- Inclination, the inclination of the semi-major axis.

These parameters are displayed in Fig. 10. For the sandpit model a residual current, the M2 and M4 components are used as input. The residual component is also given by t_tide in terms of a x- and y-velocity.

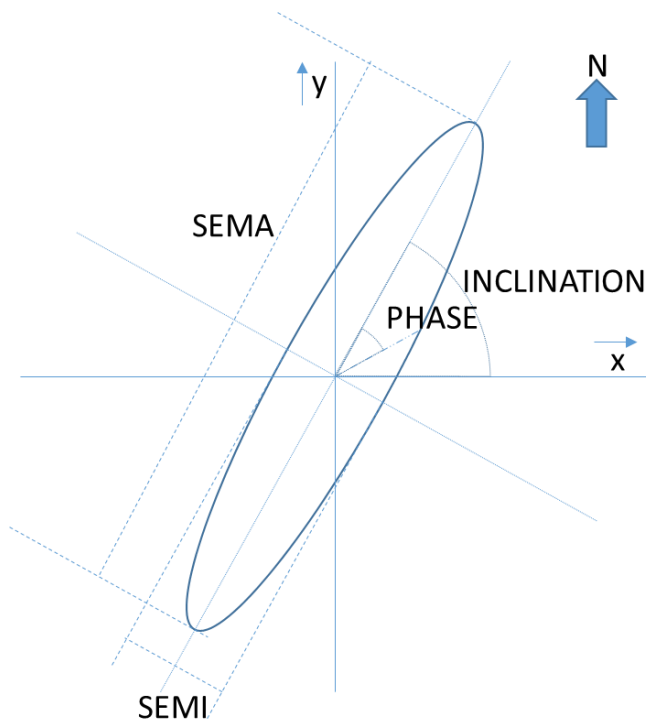


Figure 10 Tidal ellipse parameters which are used to describe a tidal ellipse signal.

In Fig. 11 it can be seen how the tidal currents over a period of 2 months (22-07-2015 – 22-09-2015, for other months see appendix 9.2) on the tidal conditions location in Fig. 6 in front of the Dutch coast are represented with the tidal ellipse which is used as input for the sandpit model

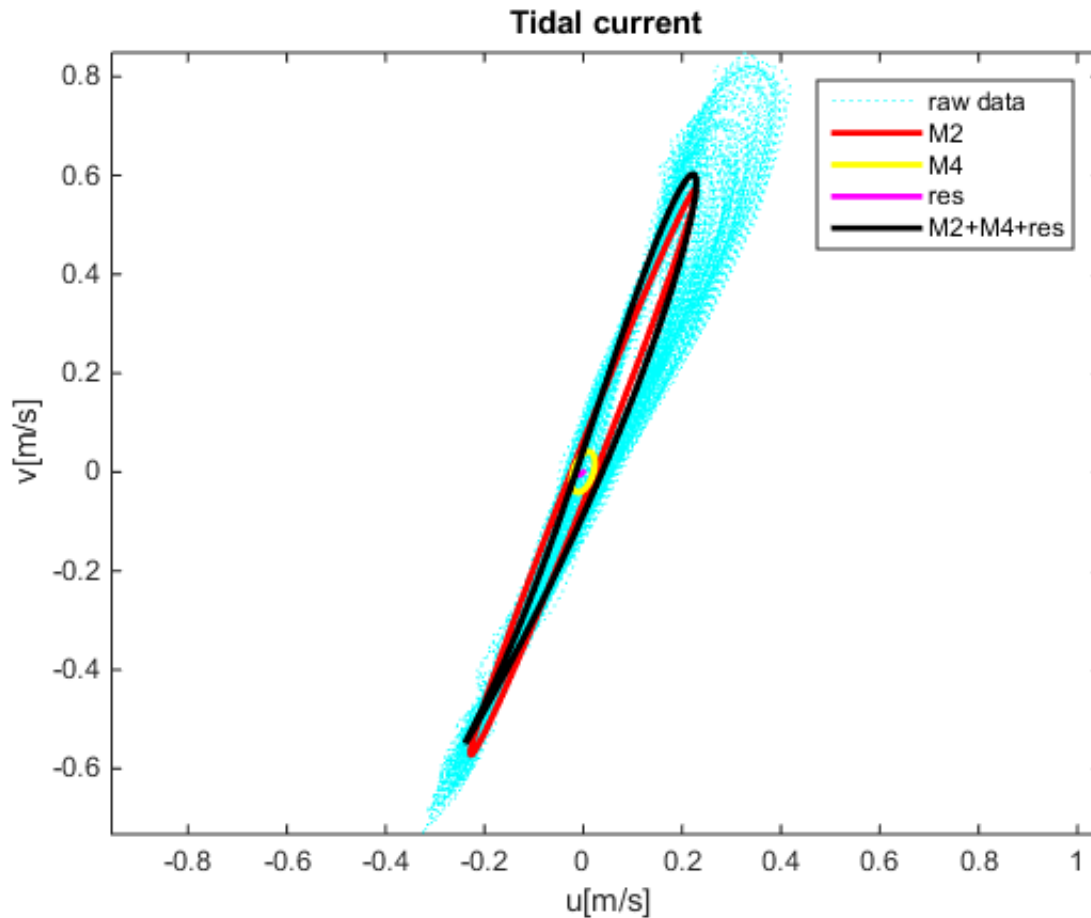


Figure 11 Representation of the raw tidal current data using tidal ellipses. Raw data obtained from the MATROOS model

The information gathered with t_tide is given in table 2

Table 2 Tidal components and residual current gathered with t_tide from raw data.

M2		M4		Residual current	
SEMA	0.616 [m/s]	SEMA	0.043 [m/s]	x	-0.007 [m/s]
SEMI	0.023 [m/s]	SEMI	0.02 [m/s]	y	-0.006 [m/s]
Inclination	68.31 [°]	Inclination	71.03 [°]		
Phase	83.84 [°]	Phase	125.65 [°]		

A scatter plot from the raw data and the computed tidal ellipse of the x- and y-velocities is made in order to assess the R-squared value, which indicates the correlation between the raw data and the computed tidal ellipse (see appendix 9.3). The R-squared values for the velocities in the x- and y-direction are $R^2_x=0,82$ and $R^2_y=0,85$ respectively. The R-squared value is sufficiently high, which indicates that the computed tidal ellipse fits the raw data well. This considering that only 2 tidal components and a residual are taken into account. The large spread in the scatter plot can be contributed to the inability of the computed tidal ellipse to describe the spring-neap cycle. This means that the lower and the higher velocities during the spring-neap cycle are neglected, especially the fact that higher flow velocities are neglected has to be taken into account when drawing conclusions. By adding the tidal components which are produced by the sun (i.e. S2 and S4 etc.) the spring-neap cycle could be reproduced. However the model only considers one tidal cycle to compute the tidally averaged sediment flux, and besides that the model is only able to take higher harmonics into account.

Storm conditions

Current dune erosion models (Vuik, 2013) use the hydraulic boundary conditions as input (See appendix 9.4). Since the hydraulic boundary conditions for the Holland Coast are only given for a recurrence period of 10,000 years, we gather boundary conditions from another source, so that we are able to get boundary conditions for different recurrence periods. The values we use in this study differ slightly from the hydraulic boundary conditions, but the difference is negligible.

On the storm conditions location in Fig. 6, water level, significant wave height, peak period, wave direction, wind speed, and wind direction data is gathered from the YM6 measurement location. The data from this measurement station is analysed and extrapolated in order to estimate hydraulic conditions for severe storms. The values for the extrapolated water level, significant wave height, and peak period can be calculated using a conditional Weibull distribution (Stijnen et al., 2005), these values are presented in Fig. 12 and Fig. 13. We choose to use the storm values corresponding to exceedance frequencies 1×10^{-2} , 1×10^{-3} , and 1×10^{-4} (1:100, 1:1.000, and 1:10.000).

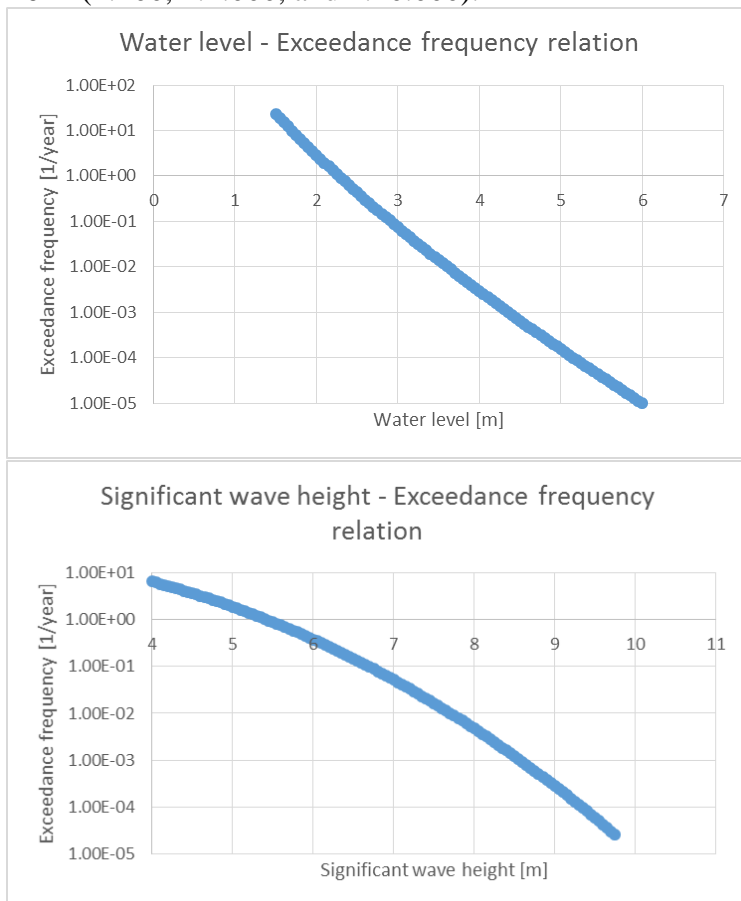


Figure 12 Water levels and significant wave heights in relation with the exceedance frequency.

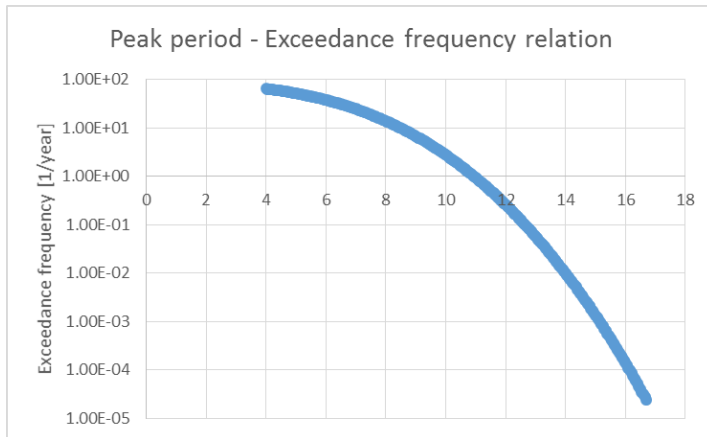


Figure 13 Relation between peak period and exceedance frequency.

The corresponding values can be found in table 3

Table 3 Storm conditions values

Exceedance frequency [1/year]	Water level [m]	Significant wave height [m]	Peak period [s]	Wind speed [m/s]
1:100	4.1	7.7	14.0	28.8
1:1.000	4.9	8.6	15.1	31.2
1:10.000	5.7	9.3	16.1	33.2

From Stijnen et al. (2005) we can also find a relation between the wind speed and the significant wave height, which is given in Fig. 14. In current dune erosion models, a post-storm equilibrium profile is calculated on the basis of deep water boundary conditions i.a. water level, wave height, and wave period (Vuik, 2013), the wind speed is not taken into account in these models, but by taking it into account in the Delft3D-WAVE model we get a more realistic set of boundary conditions compared to current models. For dunes a omni-directional (same values in every direction) relation is assumed between the wind speed and the significant wave height. Furthermore in current dune erosion evaluations, waves are assumed with an incidence angle perpendicular to the coast because of refraction (Stijnen et al., 2005).

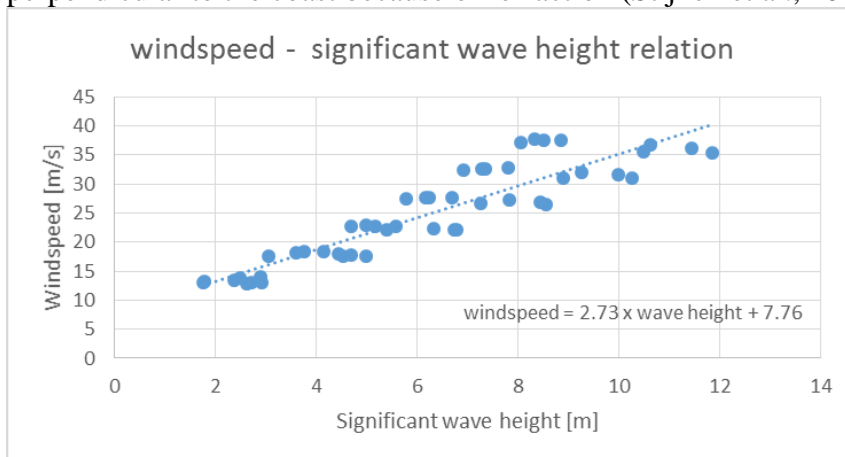


Figure 14 Relation between the wind speed and the significant wave height.

3 Sand pit model

The morphodynamic model used in this study is based on the model of Roos et al. (2008). In this study we extend the model with the possibility to use tidal ellipses with an arbitrary orientation as input for the model, instead of using a unidirectional tide.

This model will be discussed in more detail, since one goal of the thesis is to write the sand pit model in MatLab instead of Fortran.

3.1 Model geometry

The sand pit is modelled in an offshore environment, without a coastal slope. Furthermore the pit is considered as a local perturbation in an otherwise flat seabed of uniform mean water depth H^* . The pit shape is modelled roughly as a rectangular box of length L^* , width B^* , depth H_{pit}^* and edge slope length S^* (see figure 15) in a domain with domain length (we choose $L_{dom}^* = 20 \text{ km}$) in both horizontal directions (x, y) , where parameters with an asterisk $*$ denote parameters with dimension. The edge slope can either be linear or sinusoidal. The pit depth H_{pit}^* is assumed small compared to the ambient water depth H^* , which is necessary for linearization (see appendix 9.7). The pit volume is given by

$$V_{pit}^* = H_{pit}^* B^* L^*. \quad (1)$$

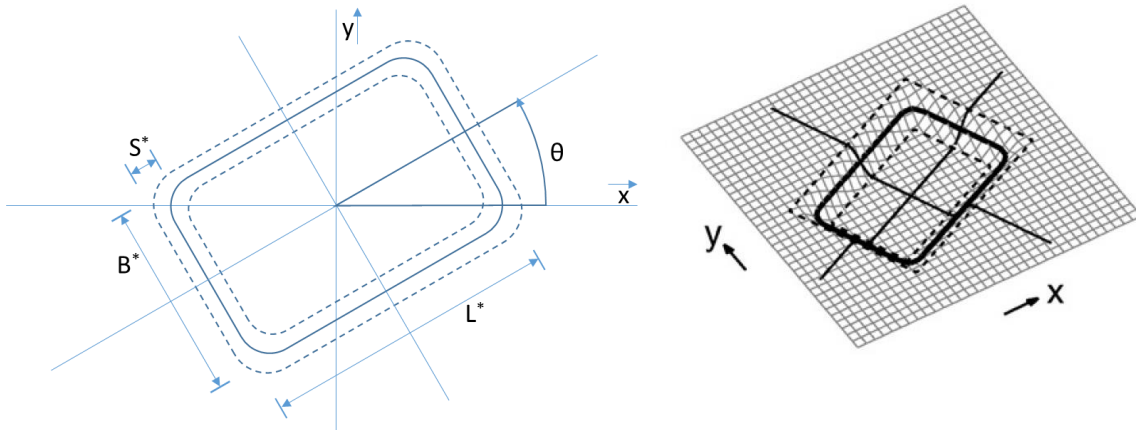


Figure 15 pit geometry parameters on the left, with a three-dimensional sketch on the right (Source: Roos et al. (2008)).

3.2 Model equations

Fluid motion is described by the nonlinear depth averaged shallow water equations, including Coriolis effects and bottom friction. No wind stress is assumed at the sea surface and the shear stress at the bottom depends linearly on the depth averaged flow velocity vector $\mathbf{u}^* = (u^*, v^*)$ according to Lorentz' linearization (Zimmerman, 1982). Horizontal momentum dispersion is neglected. The conservation of momentum and mass is expressed as follows, where the $*$ denotes parameters having dimensions, later on dimensionless quantities will be introduced:

$$\frac{\partial u^*}{\partial t^*} + u^* \frac{\partial u^*}{\partial x^*} + v^* \frac{\partial u^*}{\partial y^*} - f^* v^* + \frac{r^* u^*}{h^* + \zeta^*} = -g^* \frac{\partial \zeta^*}{\partial x^*}, \quad (2)$$

$$\frac{\partial v^*}{\partial t^*} + u^* \frac{\partial v^*}{\partial x^*} + v^* \frac{\partial v^*}{\partial y^*} + f^* u^* + \frac{r^* v^*}{h^* + \zeta^*} = -g^* \frac{\partial \zeta^*}{\partial y^*}, \quad (3)$$

$$\frac{\partial \zeta^*}{\partial t^*} + \frac{\partial}{\partial x^*} ((h^* + \zeta^*)u^*) + \frac{\partial}{\partial y^*} ((h^* + \zeta^*)v^*) = 0. \quad (4)$$

Here $f^* = 2\Omega^* \sin\phi$ is the Coriolis parameter with latitude ϕ and earth's angular velocity $\Omega^* = 7.292 \cdot 10^{-5} \text{ rad s}^{-1}$. The bottom friction is given by $r^* \mathbf{u}^*$, the linear friction coefficient r^* (in m/s) is derived using Lorentz' linearization:

$$r^* = \frac{8C_d U^*}{3\pi}, \quad (5)$$

here the velocity scale U^* (in m/s) and C_d is the dimensionless drag coefficient which varies between 0.01 and 0.001 for a shallow sea (Hulscher et al., 1993). Based on Roos et al. (2008), for $U^* = 1 \text{ m/s}$ and $C_d = 2.32 \cdot 10^{-3}$, resulting in $r^* = 1.9 \cdot 10^{-3} \text{ m/s}$.

Sediment is assumed to be mainly transported as bed load. The sediment is considered to be noncohesive and the volumetric sediment flux $\mathbf{q}^* = (q_x^*, q_y^*)$, with dimension $\text{m}^2 \text{s}^{-1}$, is modelled as

$$\vec{q}^* = \alpha^* |\vec{u}^*|^b \left(\frac{\vec{u}^*}{|\vec{u}^*|} + \hat{\lambda} \nabla^* h^* \right). \quad (6)$$

The sediment transport equation is a generalization of a class of widely used transport formulae, see Van Rijn (1989). This formula describes an increase in transport with increasing velocities and that sediment is transported easier downhill than uphill due to the bed slope coefficient $\hat{\lambda}$ (the hat denoting unscaled parameters). The $\hat{\lambda}$ term can be interpreted as the inverse of the tangent of the angle of no repose. With these angles varying between 30° to 90° the $\hat{\lambda}$ values varies from 0 to $\sqrt{3}$. The parameter α^* is the coefficient of proportionality and has the dimension $\text{m}^{-1} \text{s}^2$. The two dimensional nabla-operator $\nabla = (\partial/\partial x, \partial/\partial y)$. The exponent b is usually taken between 3 and 5. We choose $b = 3$ and $\hat{\lambda} = 2$.

Finally, the seabed topography evolves as a result of the divergence of the bed load sediment flux, i.e.

$$\frac{\partial h^*}{\partial t^*} = \frac{1}{1-\epsilon_p} \left(\frac{\partial q_x^*}{\partial x^*} + \frac{\partial q_y^*}{\partial y^*} \right), \quad (7)$$

where, $\epsilon_p = 0.4$ is the bed porosity, a dimensionless quantity.

3.3 Scaling procedure

Likewise as Roos et al. (2008) did analogous to Hulscher et al. (1993) a scaling procedure is performed, this scaling procedure can be found in appendix 9.5. The linearization of the scaled equations is given in appendix 9.7.

3.4 Basic flow conditions

The basic flow represents the flow in the reference situation without a sandpit. The reference situation is called the basic state and is denoted with subscript '0'. The basic flow of the model is described using a residual current and the M2 and M4 components of the tide as will be explained in chapter 5.1. The basic flow is given by

$$\mathbf{u}_0 = \sum_{p=-2}^{+2} \mathbf{U}_p \exp(ipt), \quad (8)$$

here the index p represents the constituents of the basic flow (see table 4) and $\mathbf{U}_p = (U_p, V_p)$ is a complex number calculated in the model according to Xu (2002). This vector contains information about the direction, phase and strength of the flow.

Table 4 Basic flow conditions

p=0	steady flow
p=-1 & p=1	together M2
p=-2 & p=2	together M4

In the basic state $h^* = H^*$ everywhere in the domain (so $h = 1$). Also q_0 is the same everywhere in the domain, due to uniformity of the flow and topography, so bed evolution is not possible.

3.5 Solution method

The solution method for the perturbed state is given in appendix 9.6

An overview of parameter values used in the 2015 sand pit model is given in table 5 and 6.

Table 5 Overview of parameter values used in the 2015 sand pit model

Quantity	Symbol	Value
Maximum flow velocity	U^*	1 m/s
Angular frequency (M2)	σ^*	$1.41 \cdot 10^{-4} \text{ rad/s}$
Length scale	l_{mor}^*	$7.1 \cdot 10^3 \text{ m}$
Latitude	ϕ	52.4°N
Coriolis Parameter	f^*	$1.16 \cdot 10^{-4} \text{ rad/s}$
Linear friction coefficient	r^*	$1.9 \cdot 10^{-3} \text{ m/s}$
Sediment flux coefficient	α^*	$4 \cdot 10^{-5} \text{ s}^2/\text{m}$
Bed slope coefficient	$\hat{\lambda}$	2
Bed porosity	ϵ_p	0.4
Dimensionless Coriolis parameter	f	0.82
Pit slope length	S	500 m
Sediment equation exponent	b	3

Table 6 Depth dependent parameter values of the 2015 sand pit model

Quantity	Symbol	$H^* = 20 \text{ m}$	$H^* = 15 \text{ m}$
Mean water depth	H^*	20 m	15 m
Dimensionless linear friction coefficient	r	0.68	0.90
Scaled bed slope coefficient	λ	$5.6 \cdot 10^{-3}$	$4.2 \cdot 10^{-3}$
Time scale ratio	$(\sigma^* T_m^*)^{-1}$	$3.33 \cdot 10^{-6}$	$4.44 \cdot 10^{-6}$

3.6 Indicators

To facilitate a quantitative comparison among different settings the following indicators are introduced:

- Area of morphodynamic influence
- Pit depth
- Pit migration.
- Radius of morphodynamic influence

This approach is similar to Roos et al. (2008), except for the pit depth and the radius of morphodynamic influence, which are new here. The area of morphodynamic influence A_{mor} is defined as the area where the difference between the actual topography and the undisturbed topography exceeds 10% of the pit depth H_{pit} . The pit depth is defined as the lowest point in the topography. Pit migration is defined as the horizontal speed of the pit's centre of 'mass', and the radius of morphodynamic influence is defined as the radius of a circle enclosing the disturbed area of morphodynamic influence, where the origin is the initial pit's centre.

4 Delft3D-WAVE model

The numerical Delft3D-WAVE model is used to simulate the evolution of wind-generated waves in coastal waters. The model computes wave propagation, non-linear wave-wave interactions and wave dissipation, for a given bottom topography and water level (Deltares, 2014).

The Delft3D-WAVE model accounts for the following physical processes:

- Wave refraction over a bottom of variable depth and/or a spatially ambient current
- Depth and current-induced shoaling
- Wave generation by wind
- Dissipation by whitecapping
- Dissipation by depth-induced breaking
- Dissipation due to bottom friction
- Nonlinear wave-wave interactions

It is important to notice that the dissipation processes result in a loss of wave energy and that wave generation by wind results in an increase in wave energy.

Wave refraction

Wave refraction is the most important process. Wave refraction is the process of the change in wave direction due to a change in velocity. In shallow water the wave speed is related to the water depth, with a decreasing water depth the wave speed decreases, this causes wave crests to align with depth contours. With different water depths due to a sand pit, waves will refract away from the pit, which is presented in Fig. 16

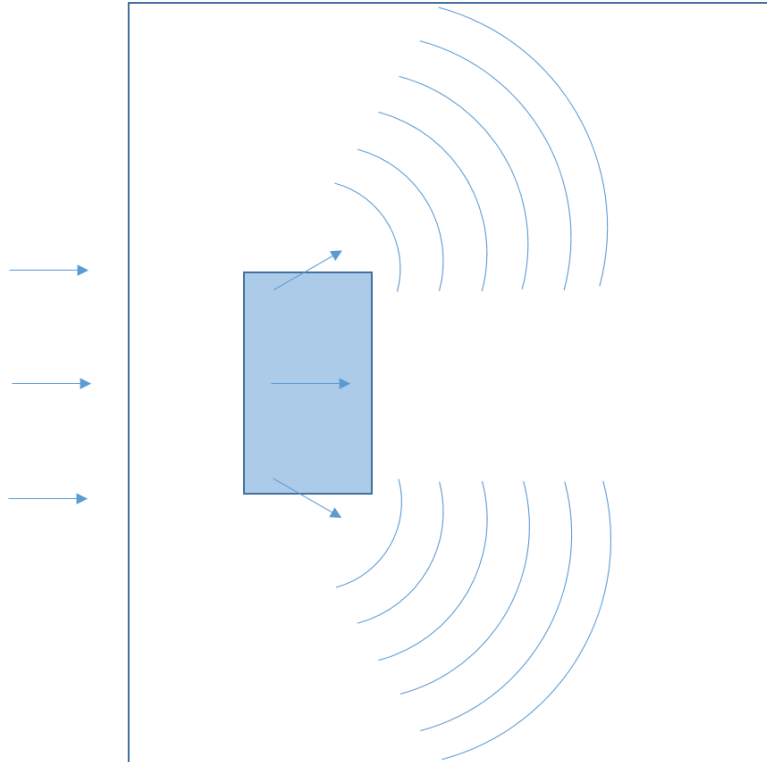


Figure 16 Refraction over a sand pit

4.1 Model schematization

The 2D schematization of the sea-bed is based on the 1D bed level profiles of the Holland Coast given in Fig. 7. A 1D schematization of the sea-bed is made based by means of the bed slopes (see Fig. 16). In this way bottom features are not taken into account, this results in a conservative approach, since these bottom features would otherwise have contributed to energy dissipation. In cross shore direction the bed level follows the schematized 1D bed level profile and in the longshore direction the depth is assumed to be uniform. The schematization starts at -22 m NAP, this is the depth of the location where the storm conditions are calculated.

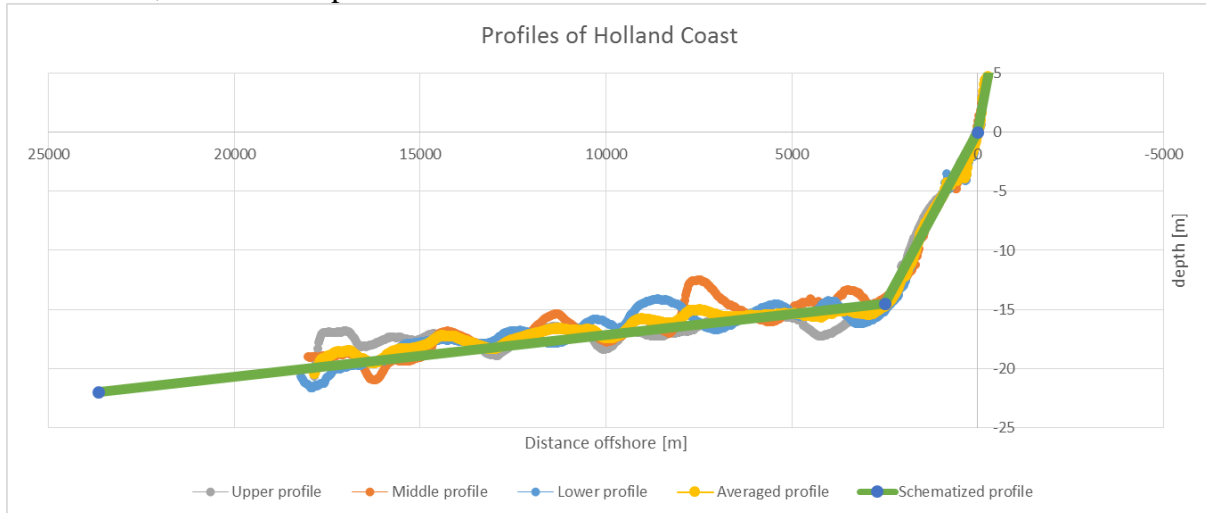


Figure 17 Schematization of the bed profile. With the coast at 0 m offshore and the established 20 m NAP depth line at 18 km offshore.

The schematization values can be found in table 7.

Table 7 schematization of the cross shore bed profile.

Distance offshore	depth [m] NAP	slope [-]
-600	10	
0	0	-60
2500	-14.5	-172
23650	-22	-2820

A 3D visualization of the 2D schematization of the bed level can be seen in Fig. 17. To eliminate edge effects, we choose the domain size in longshore direction to be three times longer than the domain size in the cross shore direction. The 2D domain consists of a grid with cells with a size of 100 x 100 m. We thus have a grid containing 243 x 729 computational cells.

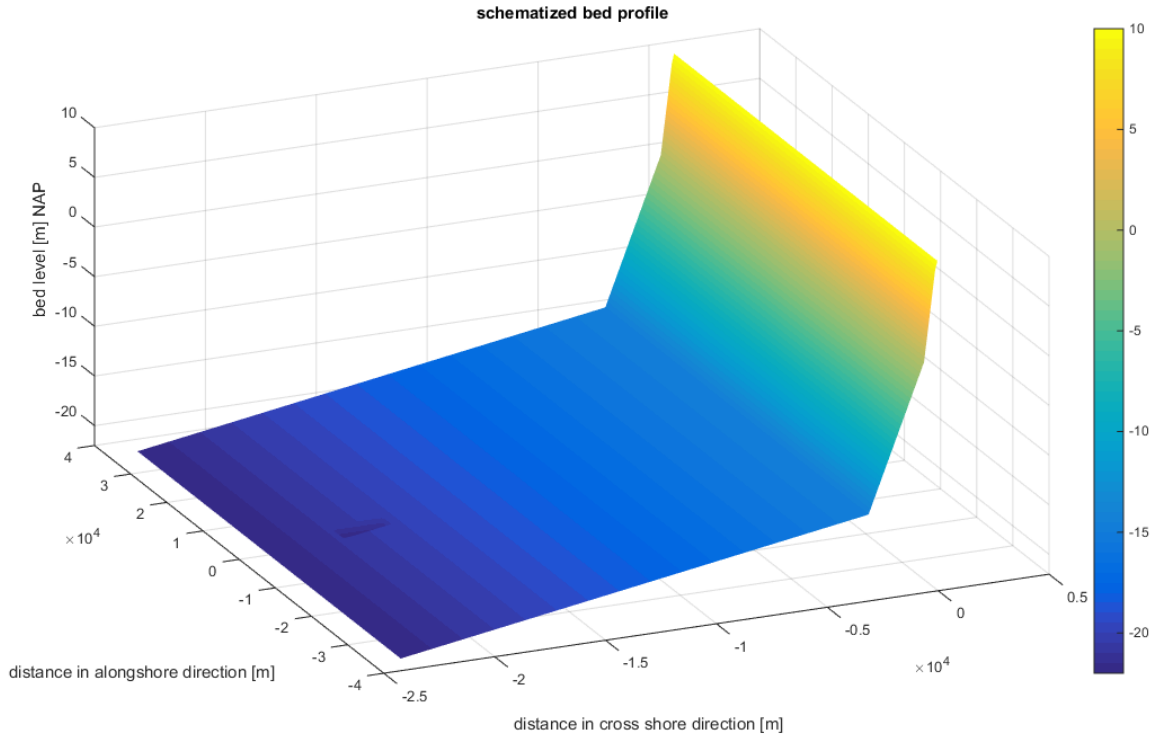


Figure 18 3D visualization of the 2D schematization of the bed level for the Delft3D-WAVE model

4.2 Model runs

The schematized profile of the Holland coast as discussed in Ch. 4.1 is used as a reference situation. We then subtract a pit geometry from this profile in order to determine the effects of the sand pit on the significant wave height. The pit geometry is defined by the pit length L , the pit width B , the pit slope length S , the pit depth H_{pit} , and the counter-clockwise orientation with respect to east θ . Since the pit is subtracted from a profile with a slope the bed level of the pit's position is not uniform, therefore we define the pit position H as the shallowest bed level in the slope where the pit is subtracted from.

The pit volume is given by $V = H_{pit}BL$. Based on the total nourishment volume in the period 2004-2014 of the coastal areas “Rijnland” and “Delfland” given in Fig. 3, which is $14.3 Mm^3$, we choose the pit volume to be $10 Mm^3$ for the determination of the effects of a small scale extraction landward of the 20 m NAP depth line. This volume is the maximum volume of a small-scale extraction. For the determination of the effects of a deeper sand pit (in terms of H_{pit}) with pit position $H = -20 m NAP$ we will look at pit depths 2, 4 and 10 m (with pit volumes 10, 20 and $50 Mm^3$).

The boundary conditions for the different storms given in table 1 are imposed on the seaward boundary. In current dune erosion assessments the wave- and wind direction are assumed to have a perpendicular angle of incidence with respect to the coast. We will also test the effect of a wave- and wind direction with an angle of incidence which has an orientation 30 degrees with respect to the perpendicular angle of incidence.

The settings of all model runs are given in table 8

Table 8 Settings for the Delft3D-WAVE model runs

Recurrence interval [year]	100	pit_ori	H [m] NAP	Vol [Mm ³]	L [km]	B [km]	A [km ²]	Hpit [m]	L/B [-]	Wind [m/s]	wavedir	winddir
Water level [m]	4.1	NaN	NaN	NaN	NaN	NaN	NaN	0	NaN	28.8	270	270
Significant wave height [m]	7.7	NaN	NaN	NaN	NaN	NaN	NaN	0	NaN	28.8	300	300
Peak period [s]	14	90	-15	10	2.74	1.83	5.00	2	1.5	28.8	270	270
		90	-17	10	2.74	1.83	5.00	2	1.5	28.8	270	270
		90	-20	10	2.74	1.83	5.00	2	1.5	28.8	270	270
		90	-15	10	2.74	1.83	5.00	2	1.5	28.8	300	300
		90	-20	20	2.74	1.83	5.00	4	1.5	28.8	270	270
		90	-20	50	2.74	1.83	5.00	10	1.5	28.8	270	270
Recurrence interval [year]	1,000	pit_ori	H [m] NAP	Vol [Mm ³]	L [km]	B [km]	A [km ²]	Hpit [m]	L/B [-]	Wind [m/s]	wavedir	winddir
Water level [m]	4.9	NaN	NaN	NaN	NaN	NaN	NaN	0	NaN	31.2	270	270
Significant wave height [m]	8.6	NaN	NaN	NaN	NaN	NaN	NaN	0	NaN	31.2	300	300
Peak period [s]	15.1	90	-15	10	2.74	1.83	5.00	2	1.5	31.2	270	270
		90	-17	10	2.74	1.83	5.00	2	1.5	31.2	270	270
		90	-20	10	2.74	1.83	5.00	2	1.5	31.2	270	270
		90	-15	10	2.74	1.83	5.00	2	1.5	31.2	300	300
		90	-20	20	2.74	1.83	5.00	4	1.5	31.2	270	270
		90	-20	50	2.74	1.83	5.00	10	1.5	31.2	270	270
Recurrence interval [year]	10,000	pit_ori	H [m] NAP	Vol [Mm ³]	L [km]	B [km]	A [km ²]	Hpit [m]	L/B [-]	Wind [m/s]	wavedir	winddir
Water level [m]	5.7	NaN	NaN	NaN	NaN	NaN	NaN	0	NaN	33.1	270	270
Significant wave height [m]	9.3	NaN	NaN	NaN	NaN	NaN	NaN	0	NaN	33.1	300	300
Peak period [s]	16.1	90	-15	10	2.74	1.83	5.00	2	1.5	33.1	270	270
		90	-17	10	2.74	1.83	5.00	2	1.5	33.1	270	270
		90	-20	10	2.74	1.83	5.00	2	1.5	33.1	270	270
		90	-15	10	2.74	1.83	5.00	2	1.5	33.1	300	300
		90	-20	20	2.74	1.83	5.00	4	1.5	33.1	270	270
		90	-20	50	2.74	1.83	5.00	10	1.5	33.1	270	270

4.3 Indicator

For the change in significant wave height we will look at 2 different areas. We will determine the change in significant wave height in the BCL zone and we will determine the change in significant wave height seaward of the BCL zone. We will look at both the absolute change as well as the relative change in significant wave height.

5 Results

In this chapter the results for the 2015 sand pit model as well as the nearshore wave model are given.

5.1 2015 Sand pit model

From the wave numbers in x- and y-direction corresponding to the largest real omega value, which corresponds to the Fourier mode with the largest growth rate (marked with a cross in Fig. 18), we find a preferred sand bank orientation of 76° counter clockwise with respect to east.

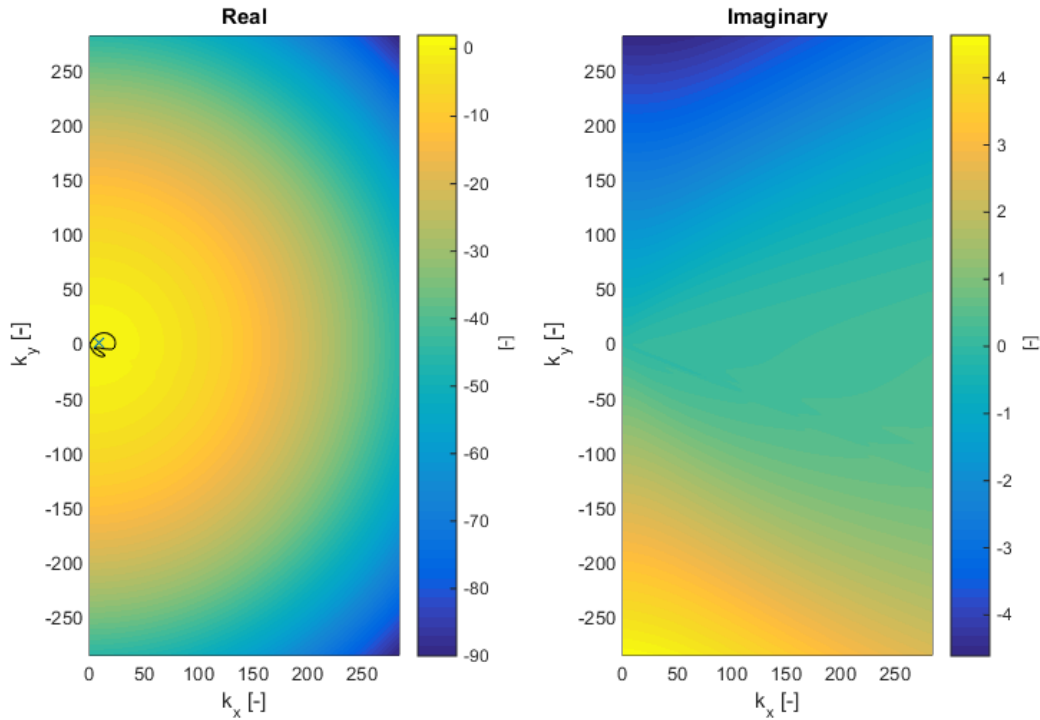


Figure 19 on the left: Real part of omega, showing growth rate per mode. The thick black line indicates $\omega_{real} = 0$. The areas inside the black line contain positive growth rates, the cross indicates the fastest growing mode. On the right: imaginary part of omega, which contributes to migration.

We will now present the results for the evolution of the sand pit topography in time. The sand pit orientations are 30° clockwise and counter clockwise with respect to the main tidal current of 70° (counter clockwise with respect to east) so that the results of sand pits with an orientation of 40° and 100° (c.c.w. w.r.t. east) respectively are presented. We will present the evolution of the sand pits with the mentioned orientations for water depths of 20 m NAP and 15 m NAP. The initial pit has a volume of 10 Mm^3 , a pit depth (H_{pit}^*) of 2 m, a pit slope length (S^*) of 500 m, and a length to-width ratio of 1.5. The other parameter values can be found in table 5 and table 6. The white contour lines in Fig. 20 to Fig. 23 indicate the area of morphodynamic influence, the threshold for the area of morphodynamic influence is a topography which exceeds 10% of the pit depth, since the length and width of the pit are defined at 50% of the pit depth (see Fig. 15) the pit dimensions seem bigger than they are.

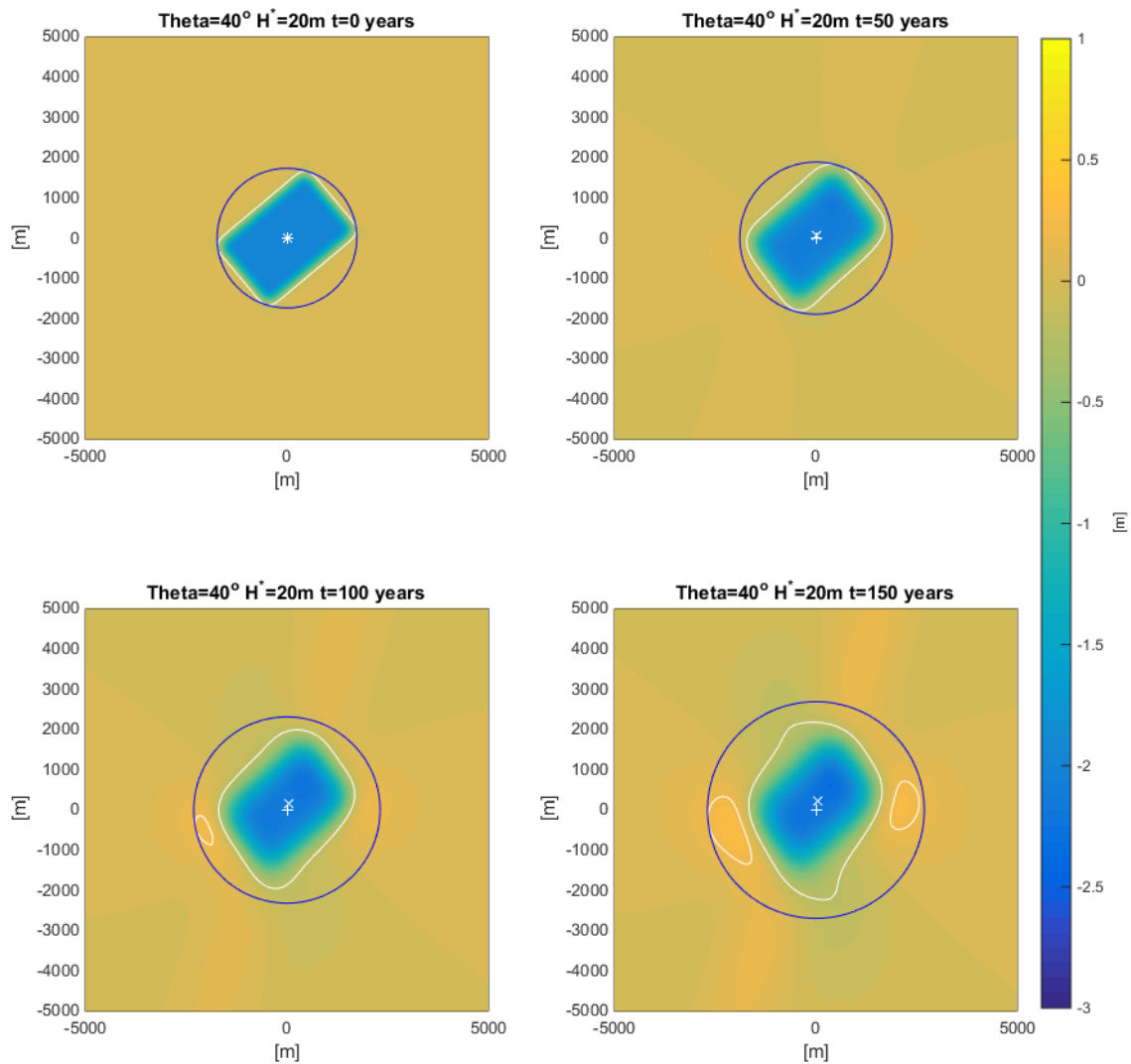


Figure 20 Evolution of the sand pit in time for a water depth of 20 m and an initial sand pit orientation of 40° (c.c.w. w.r.t. east). The centre of the initial sand pit is marked with a plus sign (+). The pit's centre of 'mass' is marked with a cross sign (x). The white contour lines indicate the area of morphodynamic influence, and the blue circle indicates the maximum radius of morphodynamic influence.

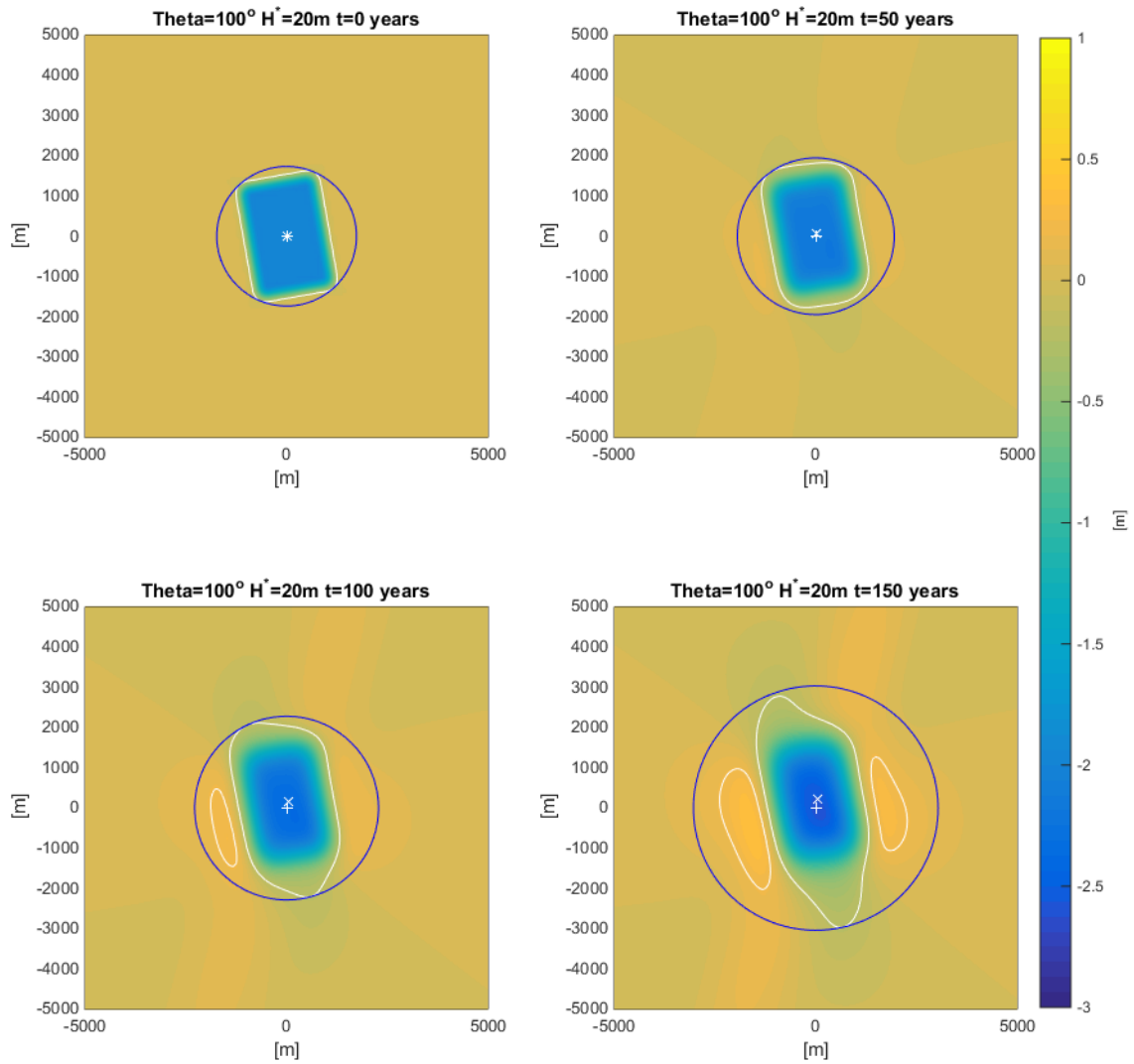


Figure 21 Evolution of the sand pit in time for a water depth of 20 m and an initial sand pit orientation of 100° (c.c.w. w.r.t. east). The centre of the initial sand pit is marked with a plus sign (+). The pit's centre of 'mass' is marked with a cross sign (x). The white contour lines indicate the area of morphodynamic influence, and the blue circle indicates the maximum radius of morphodynamic influence.

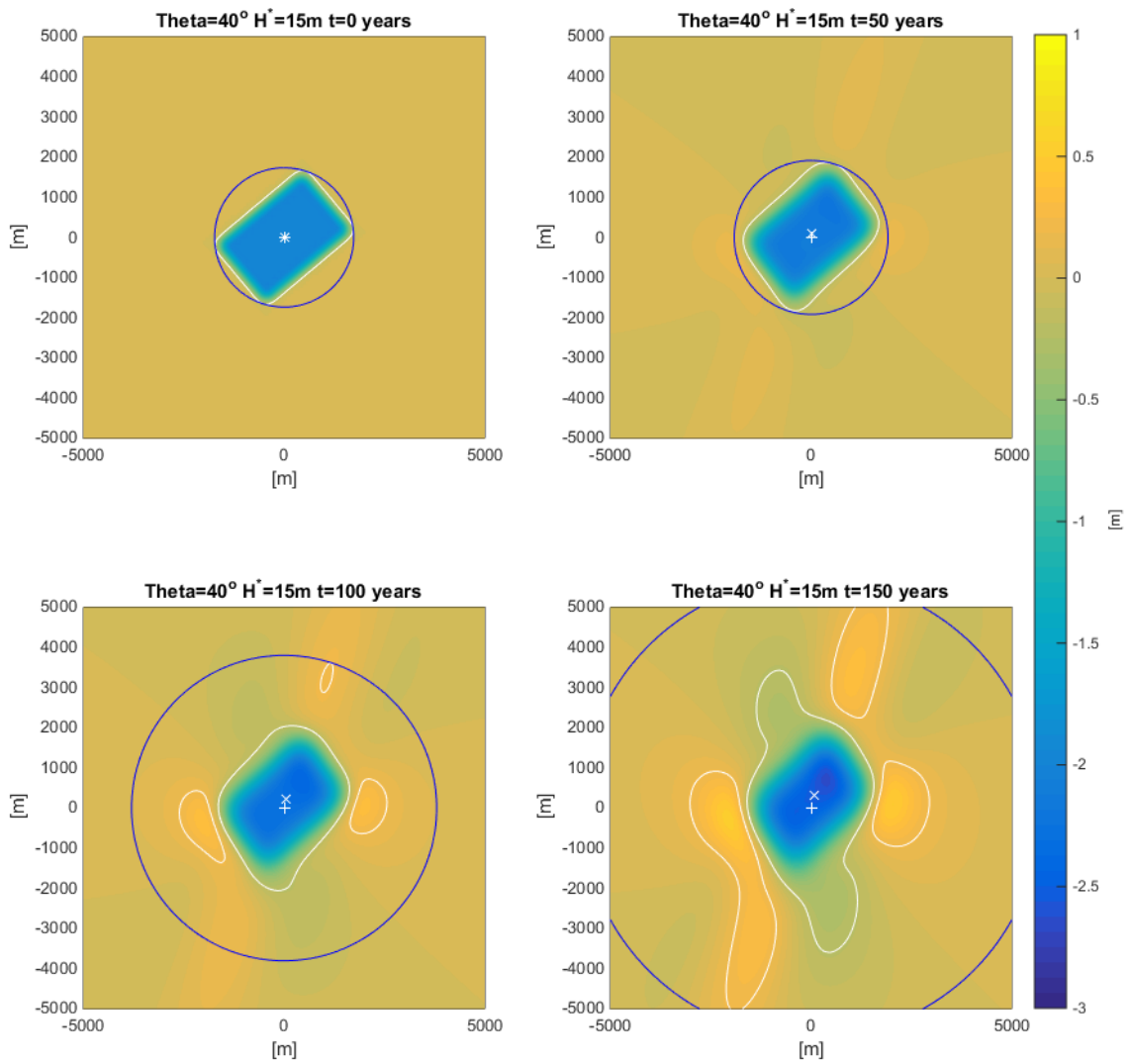


Figure 22 Evolution of the sand pit in time for a water depth of 15 m and an initial sand pit orientation of 40° (c.c.w. w.r.t. east). The centre of the initial sand pit is marked with a plus sign (+). The pit's centre of 'mass' is marked with a cross sign (x). The white contour lines indicate the area of morphodynamic influence, and the blue circle indicates the maximum radius of morphodynamic influence

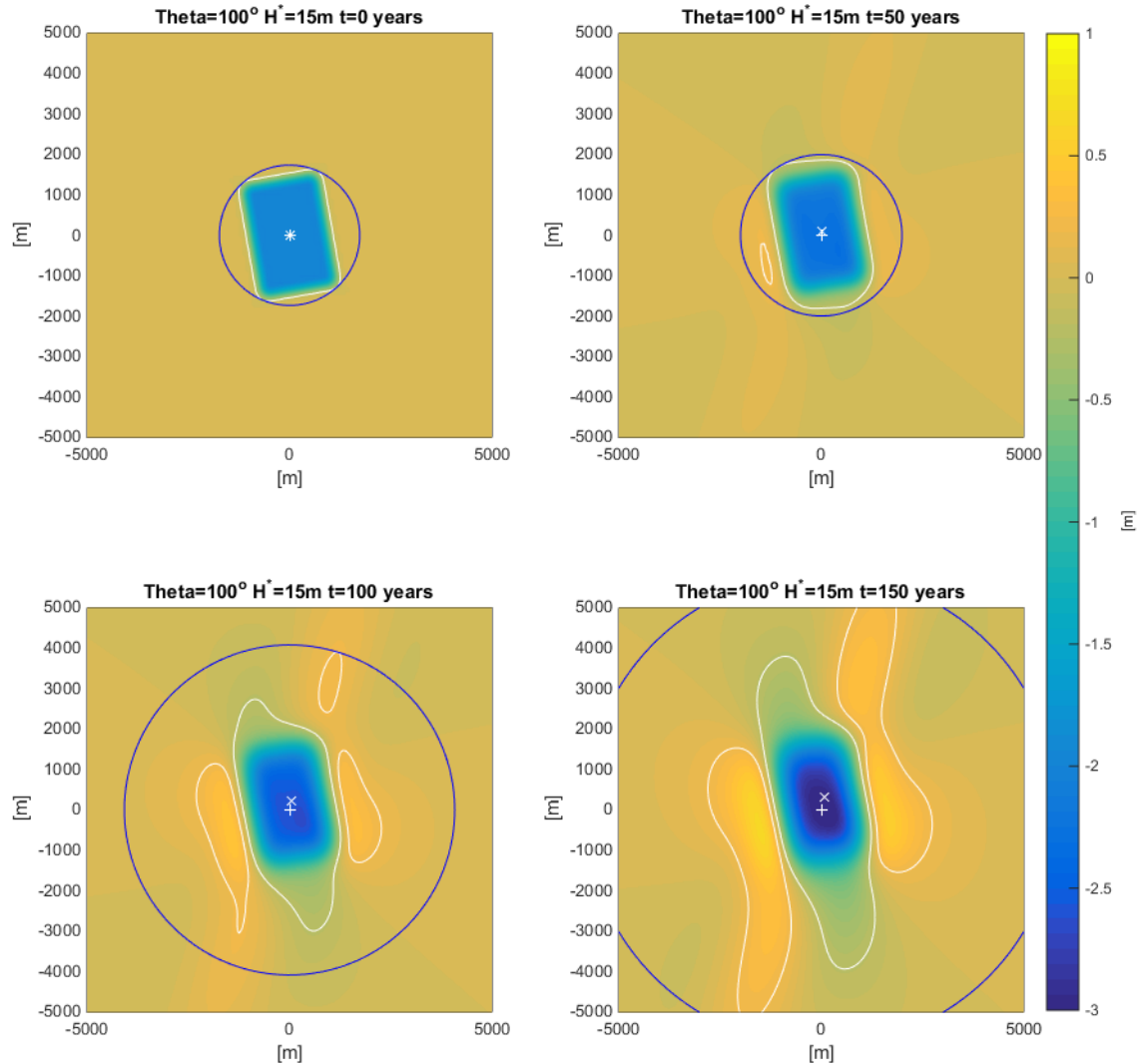


Figure 23 Evolution of the sand pit in time for a water depth of 20 m and an initial sand pit orientation of 100° (c.c.w. w.r.t. east). The centre of the initial sand pit is marked with a plus sign (+). The pit's centre of 'mass' is marked with a cross sign (x). The white contour lines indicate the area of morphodynamic influence, and the blue circle indicates the maximum radius of morphodynamic influence

When comparing Fig. 19 and Fig. 20 with Fig. 21 and Fig. 22 we can see that the morphological response for sand pits in a water depth of 15 m is much stronger than for sand pits in a water depth of 20 m. This can also be seen from the determination of the morphological time scale t_{mor} in Eq. 8. When the water depth decreases, the morphological time scale also decreases, indicating that morphological process (tidal driven sediment transport) is accelerated.

When looking at the morphological evolution after 50 years we can see that the morphological response is very small for all the model runs.

When looking at the evolution of the radius of morphodynamic influence (indicated by the blue circle) we can see that a large increase in this indicator can occur for a very small increase in the area of morphological influence (indicated by the white contour lines).

Finally we can see that the morphological response, in terms of the area of morphological influence, is strongest for the sand pits with an orientation of 110° (c.c.w. w.r.t. east).

Sensitivity analyses

We will now present the results of the sensitivity analyses. The results of the sensitivity analysis for the migration of the sand pit are not presented, since the migration was found to be 2.15 m/year in all the model runs, this agrees with the finding of Roos et al. (2008).

In Fig. 24 we can see the sensitivity analysis for the area of morphological influence. The area of morphological influence is scaled with the initial area of the sand pit. The red line indicates the main tidal current direction. We can see that the morphological response after 50 years is small for both water depths. When comparing the morphological response in time of the sand pits in 15 m water depth with the sand pits in 20 m water depth, we can see that the morphological response is larger for sand pits in 15 m water depth (especially for the response after 150 years). Finally we see that the largest increase in the area of morphological response can be found for pit directions of $\sim 70^\circ$ to 120° (c.c.w. w.r.t. east).

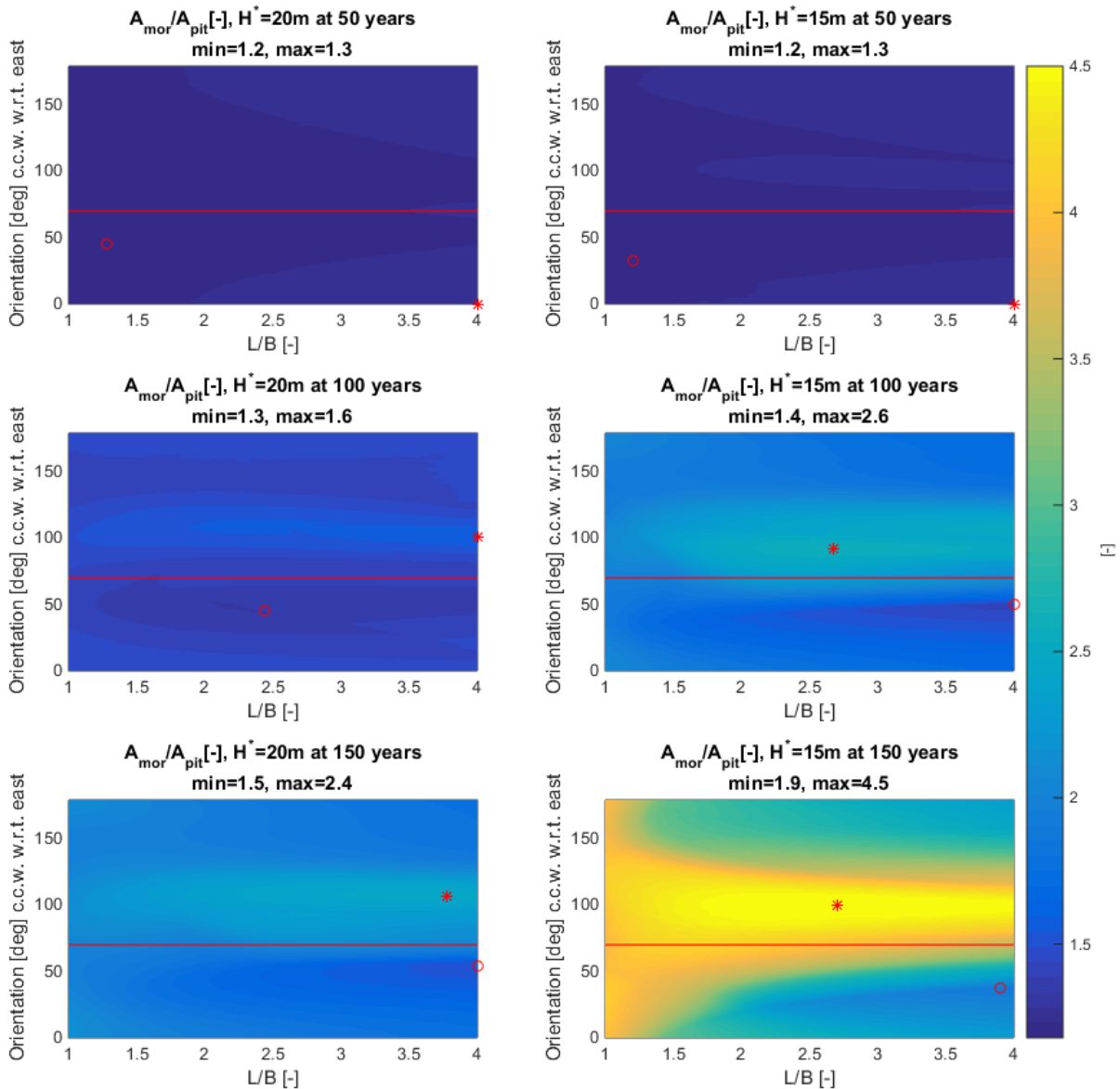


Figure 24 Sensitivity analysis for the area of morphological influence (A_{mor}) scaled with the initial area of the sand pit (A_{pit}). The red line indicates the main tidal current direction, the circle and the asterisk indicate the pit settings (in terms of L/B and orientation) with the minimum and maximum area of morphodynamic influence respectively.

In Fig. 25 the results of the sensitivity analysis for the pit deepening are presented. We can see the same results here as for the sensitivity analysis for the area of morphological response:

- Little morphological response after 50 years.
- Stronger response for the pit with a surrounding water depth of 15 m.
- Strongest morphological response for sand pit orientations ~ 70 to 120° (c.c.w. w.r.t. east).

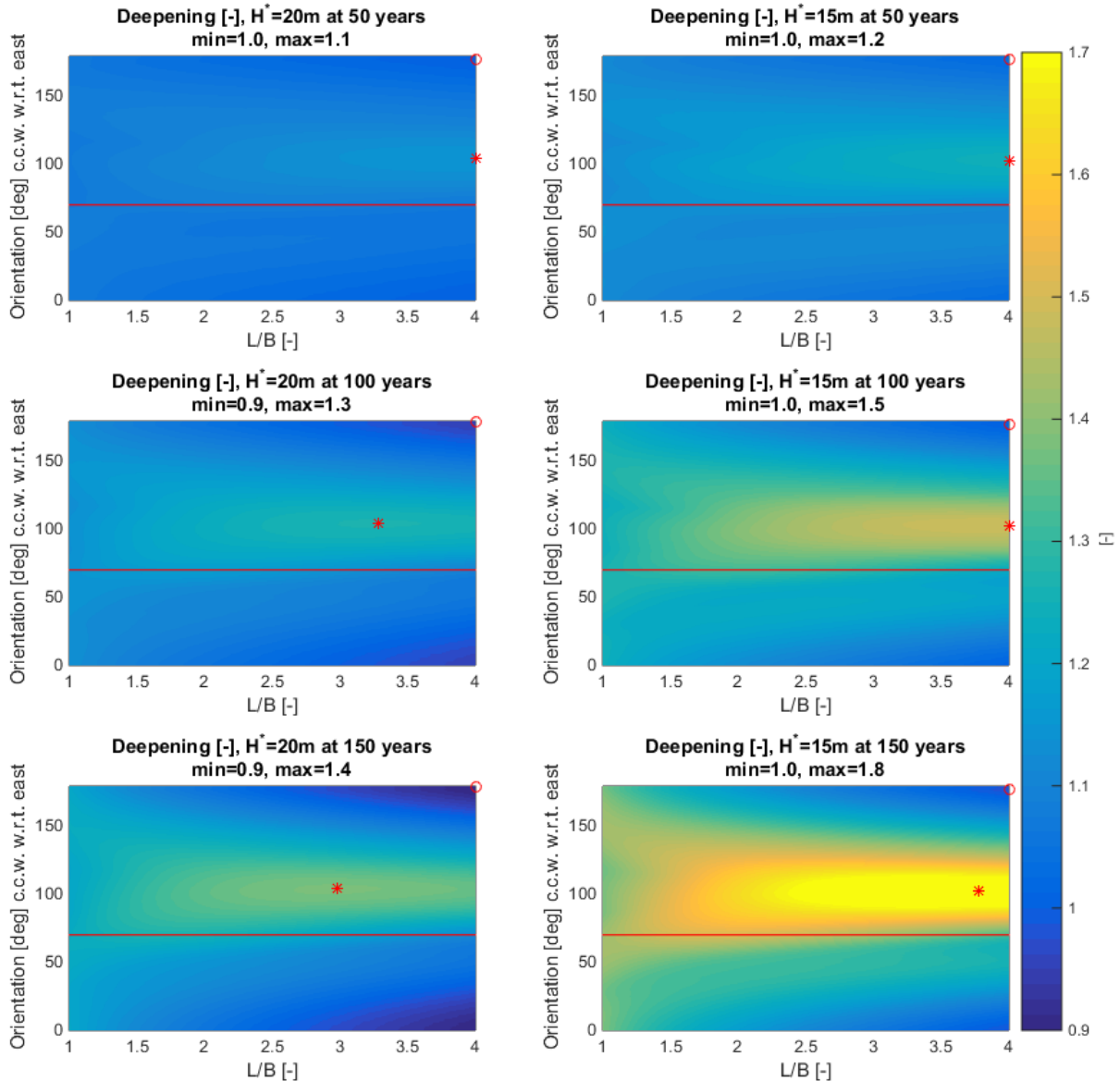


Figure 25 Sensitivity analysis for the deepening of the pit. The red line indicates the main tidal current direction, the circle and the asterisk indicate the pit settings (in terms of L/B and orientation) with the minimum and maximum area of morphodynamic influence respectively.

In Fig. 26 we the results of the sensitivity analysis for the radius of morphodynamic influence are presented. We can see little morphological response after 50 years for both pits with surrounding water depth of 20 m as for 15 m. We can also see a large increase in the radius of morphodynamic influence (from blue to yellow). The largest radius can be found for sand pits with an orientation close to the preferred sand bank orientation of 76° (c.c.w. w.r.t. east), with a deviation which depends on the point in time.

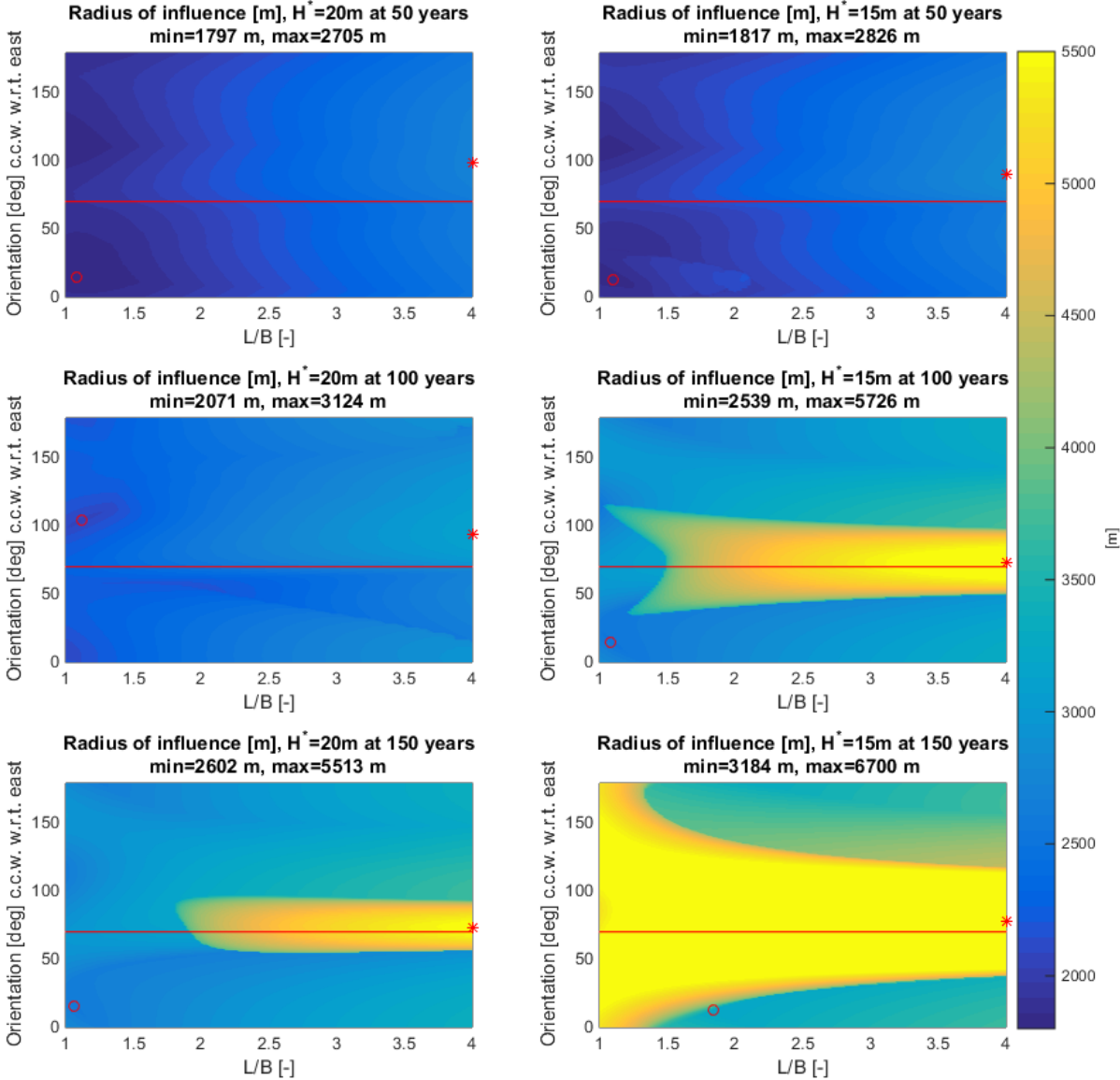


Figure 26 Sensitivity analysis for the radius of morphodynamic influence. The red line indicates the main tidal current direction, the circle and the asterisk indicate the pit settings (in terms of L/B and orientation) with the minimum and maximum area of morphodynamic influence respectively.

Concluding, we can say that: The preferred sand bank orientation is 76° (c.c.w. w.r.t. east), the morphological response is small after 50 years, that the morphological response is stronger for sand pits in shallower water, that the morphological response in terms of the area of morphological influence and the pit deepening is the largest for pits with an orientation of $\sim 70^\circ$ to 120° (c.c.w. w.r.t. east) (whereas Roos et al. (2008) found the largest response in area of morphological influence at pit orientations close to the preferred sand bank direction), that the morphological response in terms of the radius of morphodynamic influence is the largest for pits with an orientation close to the preferred sand bank orientation, and that the morphological response is more sensitive to the orientation of the sand pit than to the length to-width ratio.

5.2 Delft3D-WAVE model

In Fig. 27 the significant wave height (with a recurrence period of 100, 1,000, and 10,000 years) of the reference situation (without sand pit) is presented together with the bed level. We can see from left to right (from the -22 m NAP depth line to the dunes), that the significant wave height first increases due to shoaling and then decreases due to energy dissipation (this can be due to white capping, breaking, or bottom friction). This dissipation increases fast when the bed level increases. For the waves with an angle of incidence 30° with respect to the perpendicular incoming waves, the wave height is the same.

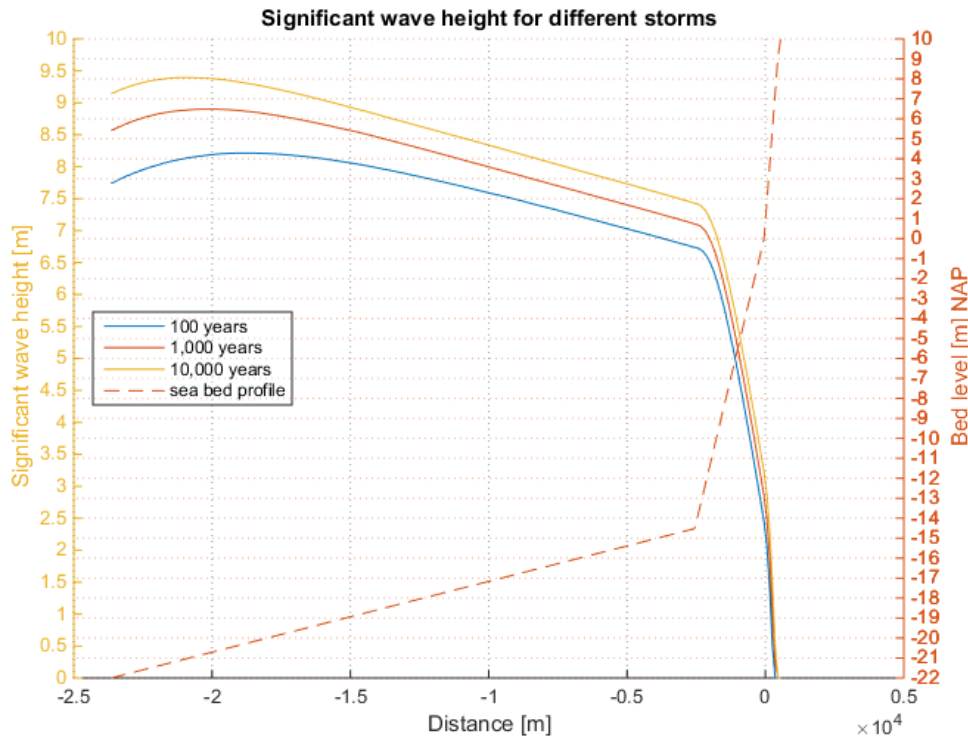


Figure 27 Significant wave height for storms with different recurrence periods presented together with the bed level.

In Fig. 28 the mean direction of the significant wave height is presented. The change in angle indicates that the wave crests are refracted to a perpendicular angle of incidence, the refraction is larger for shallower water.

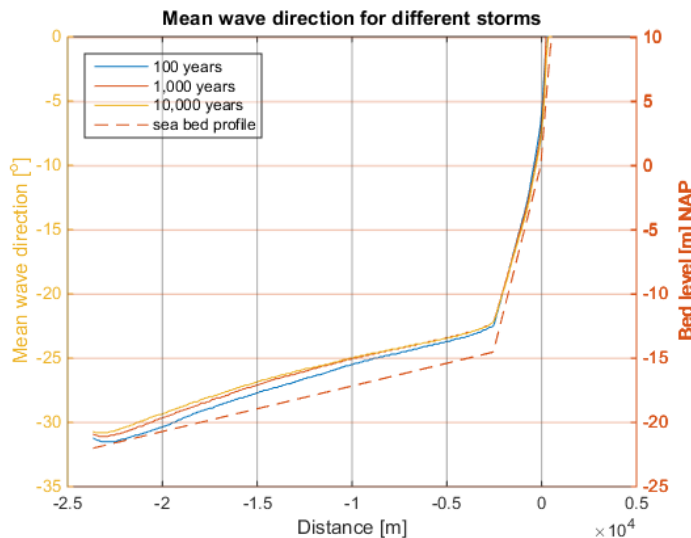


Figure 28 Mean direction of the significant wave height over the domain in cross shore direction. The wave direction is given in degrees with clockwise with respect to a perpendicular angle of incidence, which is 270° clockwise with respect to north.

We will present the results of the relative change in significant wave height for the different recurrence periods (the results are relative to the reference situation with the same recurrence period). The contour lines indicate the position of 1% increase in significant wave height. The results are quantitatively presented by means of the maximum relative and absolute change for both the BCL zone as well as the rest of the coastal foundation (established -20 m NAP to -5 m NAP). The maximum relative value does not have to correspond with the maximum absolute value.

5.2.1 Different pit locations

Fig. 29, Fig. 30, and Fig. 31 present the results of the relative change in significant wave height for a pit with a volume of 10 Mm³ and a pit depth of 2 m. The pit positions from left to right are -15 m NAP, -17 m NAP, and -20 m NAP respectively.

Recurrence period 100 years

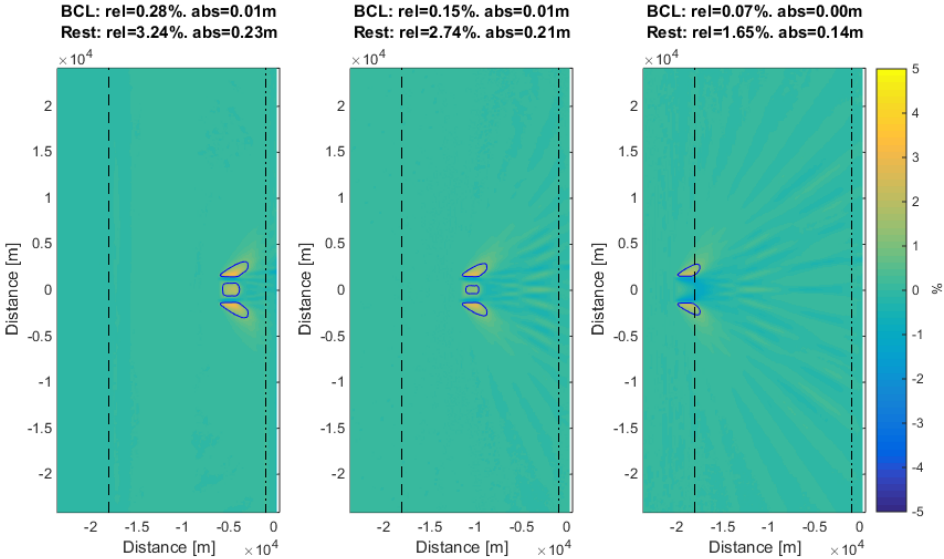


Figure 29 Relative change in significant wave height for storm conditions corresponding to a storm with a recurrence period of 100 years. From left to right the pit positions are -15 m NAP, -17 m NAP, and -20 m NAP respectively. The dashed line marks the established -20 m NAP line position, the dash-dotted line marks the -5 m NAP depth position.

Recurrence period 1,000 years

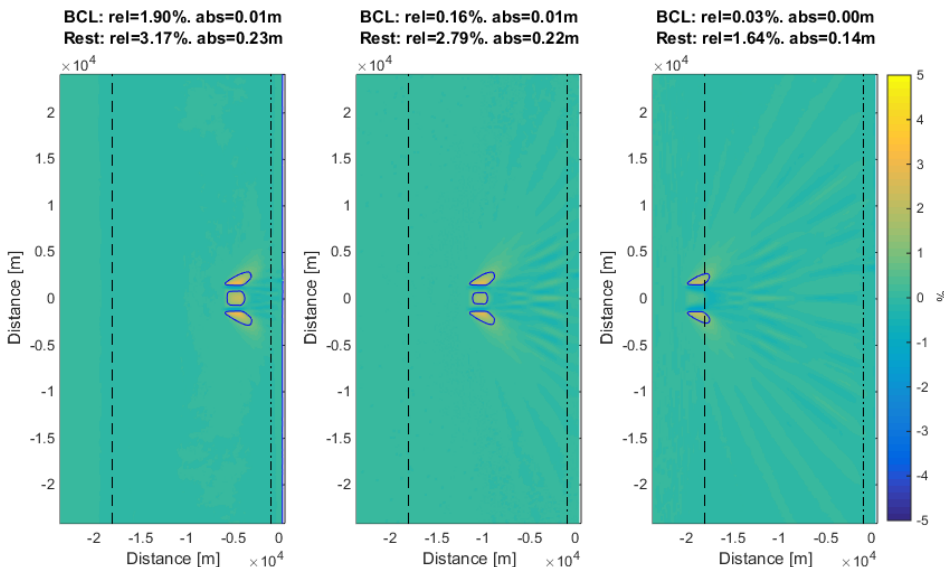


Figure 30 Relative change in significant wave height for storm conditions corresponding to a storm with a recurrence period of 1,000 years. From left to right the pit positions are -15 m NAP, -17 m NAP, and -20 m NAP respectively. The dashed line marks the established -20 m NAP line position, the dash-dotted line marks the -5 m NAP depth position.

Recurrence period 10,000 years

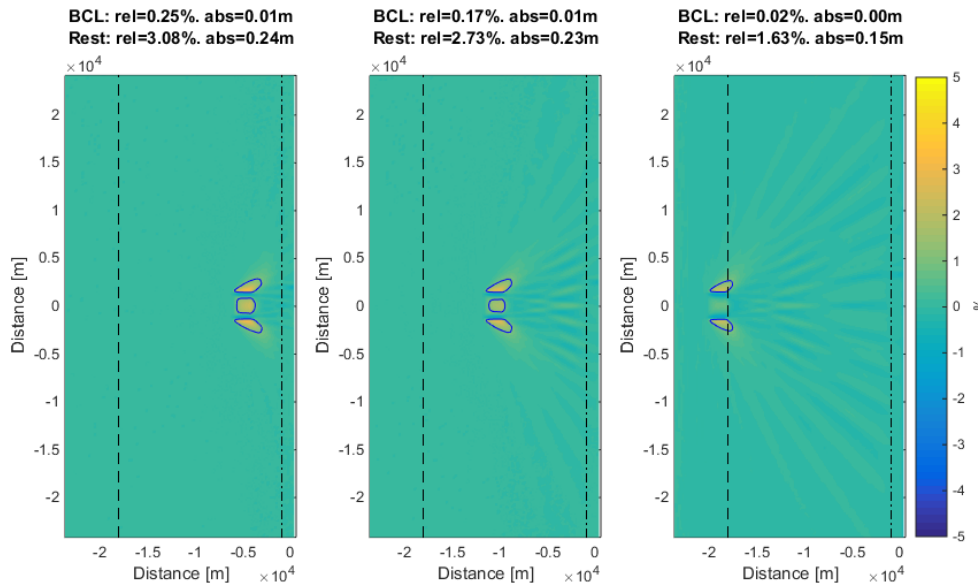


Figure 31 Relative change in significant wave height for storm conditions corresponding to a storm with a recurrence period of 10,000 years. From left to right the pit positions are -15 m NAP, -17 m NAP, and -20 m NAP respectively. The dashed line marks the established -20 m NAP line position, the dash-dotted line marks the -5 m NAP depth position.

In table 9 the values for the relative and the absolute change in the BCL zone as well as in the rest of the model are presented. We can see that the change in significant wave height (relative and absolute) in the BCL zone decreases when the sand pit is positioned farther offshore. The largest absolute change in significant wave height in the BCL zone is 0.01m and the largest relative change is 1.90%. The largest absolute change in significant wave height in the rest of the coastal foundation is 0.24 m and the largest relative change is 3.24%.

Table 9 Values for the relative and absolute change in significant wave height in the BCL zone and the rest of the domain for different pit positions, with storm conditions with a recurrence period of 100, 1,000, and 10,000 years.

Different pit locations					
Return period [years]		BCL		Rest	
	Pit location	Rel [-]	Abs [m]	Rel [-]	Abs [m]
100	-15 m NAP	0.28%	0.01	3.24%	0.23
	-17 m NAP	0.15%	0.01	2.74%	0.21
	-20 m NAP	0.07%	0.00	1.65%	0.14
1,000	-15 m NAP	1.90%	0.01	3.17%	0.23
	-17 m NAP	0.16%	0.01	2.79%	0.22
	-20 m NAP	0.03%	0.00	1.64%	0.14
10,000	-15 m NAP	0.25%	0.01	3.08%	0.24
	-17 m NAP	0.17%	0.01	2.73%	0.23
	-20 m NAP	0.02%	0.00	1.63%	0.15

5.2.2 Different pit depths.

Fig. 32, Fig. 33, and Fig. 34 present the results of the relative change in significant wave height for a pit with a position at -20 m NAP. The pit depths from left to right are 2 m, 4 m, and 10 m respectively, with pit volumes of 10Mm³, 20 Mm³, and 50 Mm³ respectively.

Recurrence period 100 years

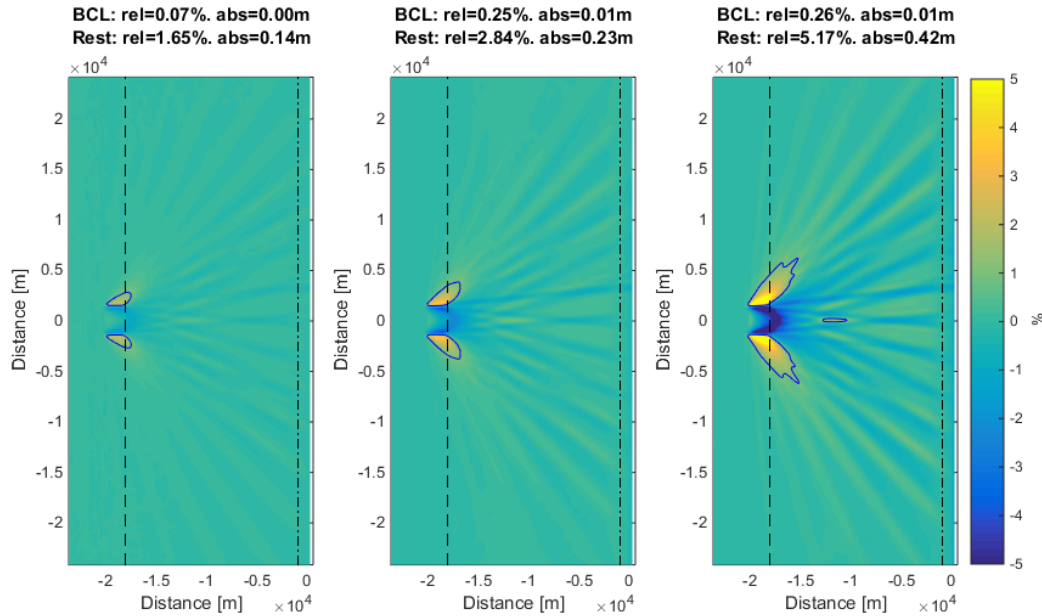


Figure 32 Relative change in significant wave height for storm conditions corresponding to a storm with a recurrence period of 100 years. From left to right the pit depths are 2 m, 4 m, and 10 m respectively, with pit volumes of 10Mm³, 20 Mm³, and 50 Mm³ respectively. The dashed line marks the established -20 m NAP line position, the dash-dotted line marks the -5 m NAP depth position.

Recurrence period 1,000 years

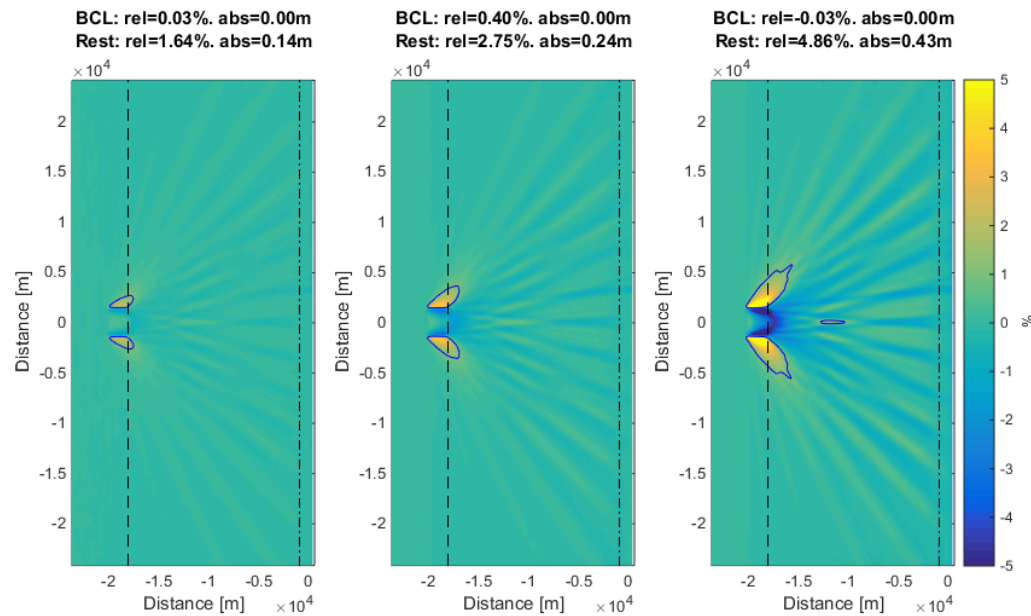


Figure 33 Relative change in significant wave height for storm conditions corresponding to a storm with a recurrence period of 1,000 years. From left to right the pit depths are 2 m, 4 m, and 10 m respectively, with pit volumes of 10Mm³, 20 Mm³, and 50 Mm³ respectively. The dashed line marks the established -20 m NAP line position, the dash-dotted line marks the -5 m NAP depth position.

Recurrence period 10,000 years

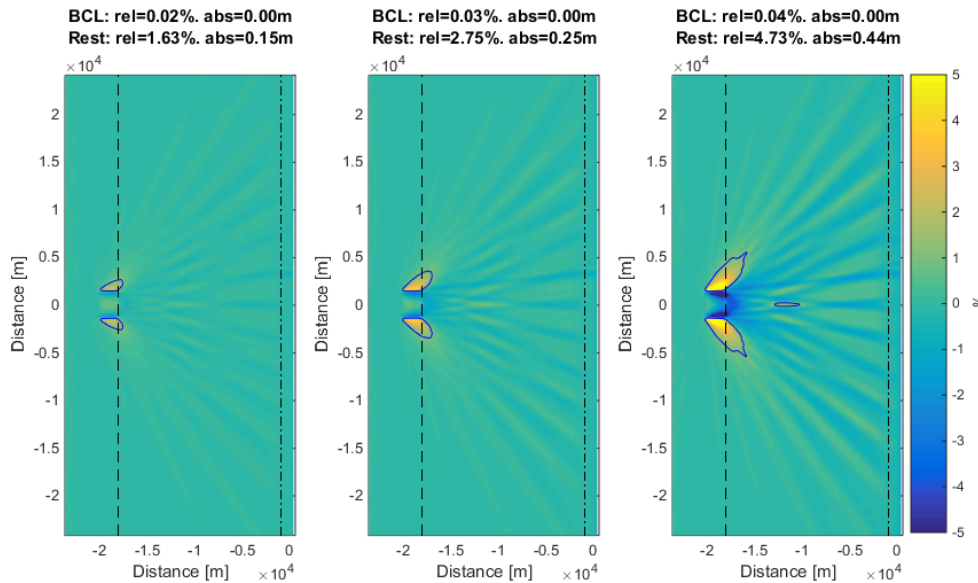


Figure 34 Relative change in significant wave height for storm conditions corresponding to a storm with a recurrence period of 10,000 years. From left to right the pit depths are 2 m, 4 m, and 10 m respectively, with pit volumes of 10Mm³, 20 Mm³, and 50 Mm³ respectively. The dashed line marks the established -20 m NAP line position, the dash-dotted line marks the -5 m NAP depth position.

In table 10 the values for the relative and the absolute change in the BCL zone as well as in the rest of the model are presented. We can see that the change in significant wave height (relative and absolute) in the BCL zone increases for deeper sand pits (in terms of the pit depth). The largest absolute change in in significant wave height in the BCL zone is 0.01 m and the largest relative change is 0.40%. The largest absolute change in the rest of the coastal foundation is 0.67 m and the largest relative change is 5.17%.

Table 10 Values for the relative and absolute change in significant wave height in the BCL zone and the rest of the domain for different pit depths, with storm conditions with a recurrence period of 100, 1,000, and 10,000 years.

Different pit depths					
Return period [years]		BCL		Rest	
	Pit depth [m]	Rel [-]	Abs [m]	Rel [-]	Abs [m]
100	2	0.07%	0.00	1.65%	0.14
	4	0.25%	0.01	2.84%	0.23
	10	0.26%	0.01	5.17%	0.42
1,000	2	0.03%	0.00	1.64%	0.14
	4	0.40%	0.00	2.75%	0.24
	10	-0.03%	0.00	4.86%	0.43
10,000	2	0.02%	0.00	1.63%	0.21
	4	0.03%	0.00	2.75%	0.36
	10	0.04%	0.00	4.73%	0.67

5.2.3 Different angle of incidence

Fig. 35, Fig. 36, and Fig. 37 present the results of the relative change in significant wave height for a pit with a position of -15 m NAP and a pit volume of 10 Mm³. The angles of incidence, for the waves and wind, from left to right are 270° and 300° (clockwise with respect to north) respectively.

Recurrence period 100 years

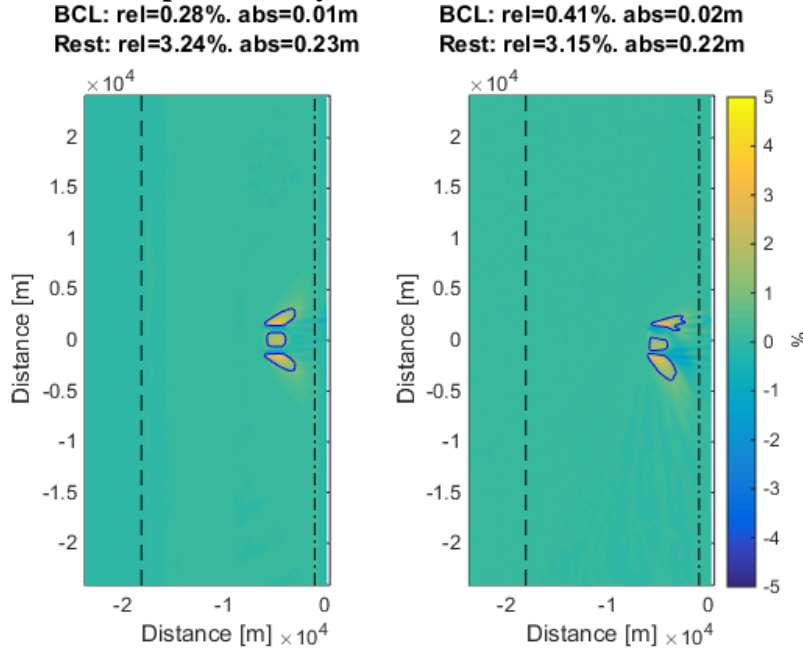


Figure 35 Relative change in significant wave height for storm conditions corresponding to a storm with a recurrence period of 100 years. From left to right the angles of incidence, for the waves and wind, are 270° and 300° (clockwise with respect to north) respectively. The dashed line marks the established -20 m NAP line position, the dash-dotted line marks the -5 m NAP depth position.

Recurrence period 1,000 years

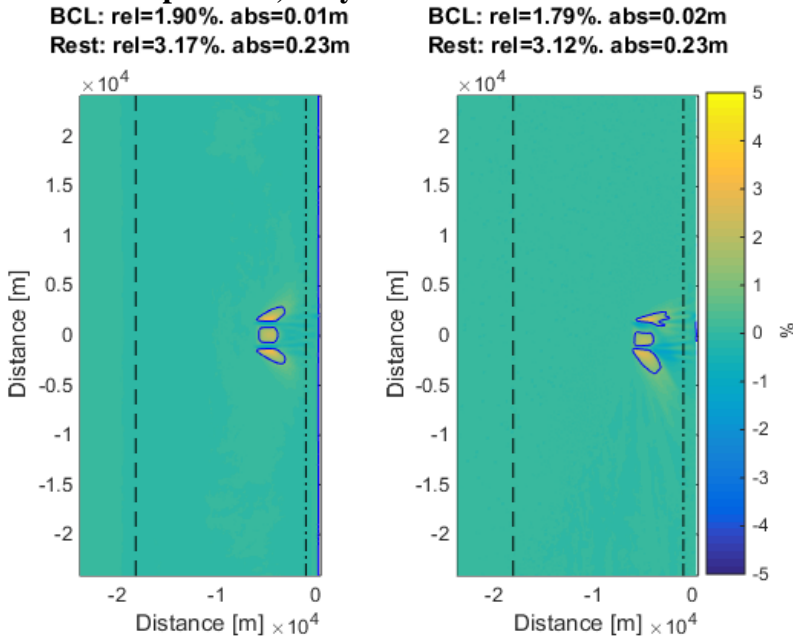


Figure 36 Relative change in significant wave height for storm conditions corresponding to a storm with a recurrence period of 1,000 years. From left to right the angles of incidence, for the waves and wind, are 270° and 300° (clockwise with respect to north) respectively. The dashed line marks the established -20 m NAP line position, the dash-dotted line marks the -5 m NAP depth position.

Recurrence period 10,000 years

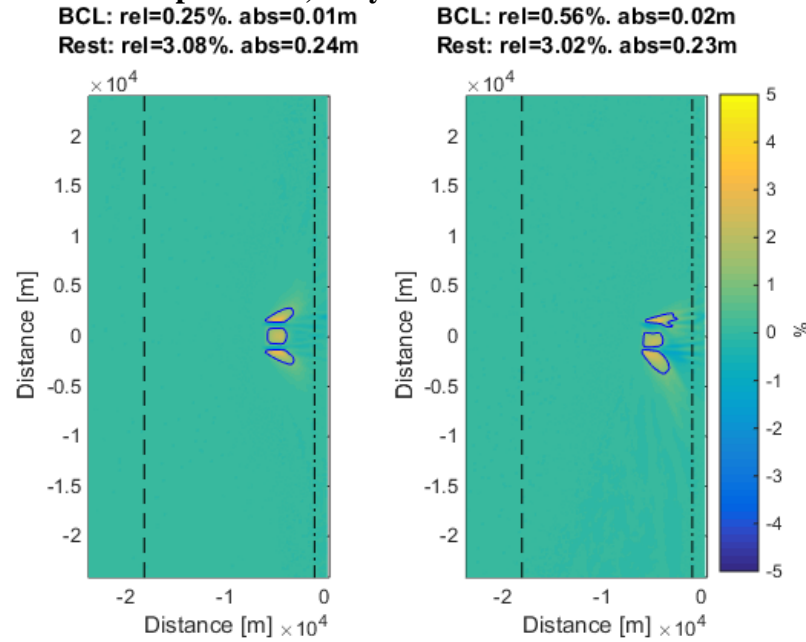


Figure 37 Relative change in significant wave height for storm conditions corresponding to a storm with a recurrence period of 10,000 years. From left to right the angles of incidence, for the waves and wind, are 270° and 300° (clockwise with respect to north) respectively. The dashed line marks the established -20 m NAP line position, the dash-dotted line marks the -5 m NAP depth position.

In table 11 the values for the relative and the absolute change in the BCL zone as well as in the rest of the model are presented. No systematic relation between the different angles of incidence or the different storm scenarios can be found. The largest absolute change in the BCL zone is 0.02 m and the largest relative change is 1.90%. The largest absolute change in the BCL zone is 0.24 m and the largest relative change is 3.24%.

Table 11 Values for the relative and absolute change in significant wave height in the BCL zone and the rest of the domain for different angles of incidence, for the waves and wind, with storm conditions with a recurrence period of 100, 1,000, and 10,000 years

Different angle of incidence		BCL		Rest	
Return period [years]	Angle [°]	Rel [-]	Abs [m]	Rel [-]	Abs [m]
100	270	0.28%	0.01	3.24%	0.23
	300	0.41%	0.02	3.15%	0.22
1,000	270	1.90%	0.01	3.17%	0.23
	300	1.79%	0.02	3.12%	0.23
10,000	270	0.25%	0.01	3.08%	0.24
	300	0.56%	0.02	3.02%	0.23

Concluding, we can say that a refraction pattern can be found for all model runs. This occurs because the water depth in the sand pit is larger than the water depth outside of the pit, which causes the waves on top of the pit to refract away from the pit. The refraction spreads wave energy, this leads to lower significant wave heights landward of the sand pit. Refraction is larger for larger differences between the bed level inside the pit and the bed level outside the pit. The largest absolute and relative change in significant wave height in the BCL zone are 0.02 m and 1.90% respectively. The largest absolute and relative change in significant wave height in the rest of the coastal foundation are 0.67 m and 5.17% respectively. Note that the largest value for absolute and relative change do not have to correspond.

6 Discussion

It is not feasible to validate the outcomes of the 2015 sand pit model, this has to do with the little available field data for validation as well as the number of assumptions made in the model. However Peters and Hulscher (2006) think that validation of these kind of models will not solve the problem decision makers deal with, and that although invalidated, decision makers can use the model results by using them as early warning signals.

The model considers a sand pit in an uniform offshore environment, whereas in reality ambient bed forms are present as well as a slope towards the coast. The model also considers a uniform friction parameter, indicating a uniform grainsize of the sediment. In reality different grain sizes may be present at different parts of the bottom. However the 2015 sand pit model can very well be used as a quick tool to analyse the effects of varying the physical characteristics as well as the pit geometry.

The 2015 sand pit model is linearized with respect to the bed amplitude and does not take higher order effects into account, the model is therefore unable to damp the growth rate and reach an equilibrium. Actual bed forms are in equilibrium and trying to validate the model with an actual topography is therefore meaningless.

The 2015 sand pit model is capable of determining the preferred sand bank direction, whereas in front of the Holland coast (See Fig.8) bed features are present with another orientation. These bed features are shoreface connected ridges. Shoreface connected ridges are present in storm-dominated inner shelves (Calvete et al, 2001). Because the 2015 sand pit model only takes tidal driven sediment transport into account these bed features cannot be modelled. The applicability of the 2015 sand pit model in this area is therefore questionable.

Also the 2015 sand pit model uses a depth averaged flow approach, the model is thus unable to simulate smaller bed forms than sand banks, such as tidal sand waves, since these smaller bed forms require a model that resolves vertical variations in flow.

For the calculation of the morphodynamic time scale in the 2015 sand pit model, we used the same value for the sediment flux coefficient α^* as Roos et al. (2008). It has to be noted that the morphodynamic time scale is just used to give an indication about the time scales.

The Delft3D-WAVE model uses a uniform bed profile in the alongshore direction, the results are therefore nearly symmetrical (not fully symmetrical because of the error margin in the numerical conversion) for symmetrical sand pits (provided that the angle of incidence for the wind and waves is perpendicular to the coast). Modelling with real topographical data could result in different outcomes.

The Delft3D-WAVE model only calculates the hydrodynamics, while during a storm the pit geometry could change a lot. It would thus be recommended to also model the morphodynamic evolution of a sand pit during a storm.

In the schematization of the sea bed for the Delft3D-WAVE model, a strong transition in the bed slope at 15 m NAP depth is present. This abrupt change triggers a strong increase in energy dissipation. It would be better to use a smoother transition.

7 Conclusions and Recommendations

To conclude this study, the research questions will be answered and recommendations for further research will be given.

7.1 Conclusions

First, we will answer the sub-questions.

1. What is the minimal increase in area of morphodynamic influence?
After 50 years, the increase in area of morphodynamic influence is 1.2 for both pits located in a surrounding water depth of 20 m as well as 15 m. After 150 years, the increase in area of morphodynamic influence is 1.5 and 1.9 for pits in a surrounding water depth of 20 m and 15 m respectively.
2. What is the minimal pit deepening value?
After 50 years the minimal pit deepening value is 1.0 for both pits located in a surrounding water depth of 20 m as well as 15 m. After 150 years, the minimal pit deepening value is 0.9 and 1.0 for pits in a surrounding water depth of 20 m and 15 m respectively.
3. What is the minimal radius of morphodynamic influence?
After 50 years the minimal radius of morphodynamic influence is 1797 m and 1817 m for pits in a surrounding water depth of 20 m and 15 m respectively. After 150 years the minimal radius of morphodynamic influence is 2602 m and 3184 m for pits in a surrounding water depth of 20 m and 15 m respectively.
4. What is the value for migration of the pit's centre of 'mass'?
The value for migration of the pit's centre of 'mass' for the tidal conditions used in this study is 2.15 m/year for all model runs, this agrees with the findings of Roos et al. (2008).
5. What are the effects of a deeper sand pit in terms of morphodynamic influence?
The 2015 sand pit model is linearized w.r.t. the bed amplitude and will therefore give the same values as given in sub-questions 1, 2, and 3 for a deeper sand pit.
6. What are the effects of a deeper sand pit in terms of significant wave height?
A deeper sand pit will not cause significant changes to the significant wave height in the BCL zone. In the rest of the coastal foundation a maximum increase of 5.17% is found for a pit directly positioned at the established -20 m NAP depth line with a pit depth of 10 m corresponding to a pit volume of 50 Mm³. However these effects are very local.

Concluding, we will answer the main research questions.

1. What is the effect of a large scale extraction within the 2 km zone seaward of the established 20 m NAP depth line in front of the Holland Coast?
The morphodynamic effect of a large scale extraction is the same as a small scale extraction due to the linearity of the model. It can be said for the tidal conditions used in this study and given that sediment transport is tidal driven, that the morphodynamic effects are small after 50 years. After 50 years, the shape of the pit is nearly the same as the initial pit.
In terms of significant wave height a large scale extraction does not result in a significant change in the BCL zone, but in the rest of the coastal foundation a maximum relative and absolute increase of 5.17% and 0.67 m respectively is found, but this increase is very local.

2. What is the effect of sand extractions landward of the established -20 m NAP depth line in front of the Holland Coast?

In terms of morphodynamic effect, the morphodynamic time scale decreases with decreasing surrounding water depth in the 2015 sand pit model, so morphodynamic effects occur at a faster rate. However morphodynamic effects are still small after 50 years and the shape of the pit is nearly the same as the initial sand pit.

In terms of significant wave height, a maximum relative and absolute increase of 1.90% and 0.02 m respectively in the BCL zone is found. In the rest of the coastal foundation a maximum relative and absolute increase of 3.24% and 0.23 m respectively is found.

Although the model outcomes cannot be validated, the outcomes of both models show little effects in both morphodynamic effects after 50 years as well as for the significant wave height with the used model settings.

7.2 Recommendations

However more research will have to be performed in which the following recommendations should be applied:

- Include non-linear effects in the 2015 sand pit model to include slowing down of growth.
- Test the morphological response for a non-uniform surrounding sea bed.
- Add a sloping bed in the 2015 sand pit model.
- Calculate the cross-shore distance of influence for the significant wave height.
- Test the response of the significant wave height with a less schematized topography.
- Include the morphodynamic evolution of a sand pit during storm conditions.

8 References

- Delta Programme. (n.d.). *Compass for the Coast*.
- Calvete, D., Walgreen, M., de Swarf, H. E., & Falqués, A. (2001). A model for sand ridges on the shelf: Effect of tidal and steady currents. *Journal of Geophysical Research C: Oceans*, 106(5), 9311–9325. doi:10.1029/2001JC900001
- Deltares. (2014). Delft3D-WAVE, User Manual, 1–226.
- Dorst, L. L. (2009). *Estimating Sea Floor Dynamics in the Southern North Sea to Improve Bathymetric Survey Planning*. Retrieved from doi:10.3990/1.9789036528788. PhD Thesis
- Elias, E., & Bruens, A. (2013). Beheerbibliotheek Noord-Holland. *Deltares*, (1207724-004).
- Geomorfologie NCP. (n.d.). Retrieved October 30, 2015, from <http://www.noordzeeloket.nl/ruimtelijk-beheer/noordzee-atlas/watersysteem/geomorfologie.aspx/>
- Giardino, A., Santinelli, G., & Bruens, A. (2012). The state of the coast (Toestand van de kust). *Deltares*, (1206171-003), 130.
- Hulscher, S. J. M. H., de Swart, H. E., & de Vriend, H. J. (1993). The generation of offshore tidal sand banks and sand waves. *Continental Shelf Research*, 13(11), 1183–1204. doi:10.1016/0278-4343(93)90048-3
- Korrelgrootte zand. (n.d.). Retrieved October 30, 2015, from <http://www.noordzeeloket.nl/ruimtelijk-beheer/noordzee-atlas/watersysteem/korrelgrootte-zand.aspx>
- Maljers-Oosterwijk, D., Vonhögen-Peeters, L., van Heteren, S., Marges, V., Stafleu, J., & Wiersma, A. (2014). De update van het delfstoffeninformatiesysteem voor het NCP. *Deltares*, (1205135-002).
- Ministerie van Verkeer en Waterstaat. (1991). ONTGRONDINGENPLAN NOORDZEE / MILIEU-EFFECT RAPPORT (RON / MER), (c10130).
- Ministerie van Verkeer en Waterstaat. (2004). Regionaal Ontgrondingenplan Noordzee.
- Ministerie van Verkeer en Waterstaat. (2007). Hydraulische Randvoorwaarden primaire waterkeringen; voor de derde toetsronde 2006-2011 (HR2006).
- Pawlowicz, R., Beardsley, B., & Lentz, S. (2002). Classical tidal harmonic analysis including error estimates in MATLAB using T_TIDE. *Computers & Geosciences*, 28(8), 929–937. doi:10.1016/S0098-3004(02)00013-4
- Peters, B. G. T. M., & Hulscher, S. J. M. H. (2006). Large-scale offshore sand extraction: What could be the results of interaction between model and decision process? *Ocean & Coastal Management*, 49(3-4), 164–187. doi:10.1016/j.ocecoaman.2006.02.007
- Rijkswaterstaat. (2014). Kustlijnkaarten 2015.
- Roos, P. C., & Hulscher, S. J. M. H. (2003). Large-scale seabed dynamics in offshore morphology: Modeling human intervention. *Reviews of Geophysics*, 41(2), 1010. doi:10.1029/2002RG000120
- Roos, P. C., Hulscher, S. J. M. H., & de Vriend, H. J. (2008). Modelling the morphodynamic impact of offshore sandpit geometries. *Coastal Engineering*, 55(9), 704–715.

doi:10.1016/j.coastaleng.2008.02.019

Stijnen, J. W., Duits, M. T., & Thonus, B. I. (2005). Diepwaterrandvoorwaarden. *HKV*, (PR841.40).

van Koningsveld, M., & Mulder, J. P. M. (2004). Sustainable Coastal Policy Developments in The Netherlands. A Systematic Approach Revealed. *Journal of Coastal Research*, 20(2), 375–385. doi:10.2112/1551-5036(2004)020[0375:SCPDIT]2.0.CO;2

Vonhögen-Peeters, L., Van Heteren, S., Bruens, A., & Stafleu, J. (2012). Zandwinstrategie : naar een beslissingsondersteunend systeem voor mariene zandwinning. *Deltares*, (1205135-000).

Vuik, V. (2013). Probabilistische toetsing van duinen. *HKV*, (PR2632.10).

Xu, Z. (2002). Ellipse parameter conversion and velocity profiles for tidal currents in Matlab.

Zimmerman, J. T. F. (1982). On the Lorentz linearization of a quadratically damped forced oscillator. *Physics Letters*, 89A(3), 123–124. doi:10.1016/0375-9601(82)90871-4

9 Appendix

9.1 Future sand extraction scenarios

Scenario	Start	Total need for sand (Mm ³ /year)	Nourishments	Expected sea level rise	Commercial need for sand (Mm ³ /year)
0 ('basic')	2010	12+13=25	small	0 mm/y	13
1 ('low')	2015	20+13=33	big	2 mm/y	13
2 ('medium')	2025	40+25=65	big	4 mm/y	25
3 ('high')	2050	85+25=110	big	13 mm/y	25

Figure 38 Different future sand extraction volumes, including extractions for the commercial use of sand (Vonhögen-Peeters et al., 2012).

9.2 Tidal current data

Table 12 tidal current data

22 July - 22 sep 2015						
M2		M4			Residual current	
SEMA	0.616 [m/s]	SEMA	0.043 [m/s]	x		-0.007 [m/s]
SEMI	0.023 [m/s]	SEMI	0.02 [m/s]	y		-0.006 [m/s]
Inclination	68.31 [°]	Inclination	71.03 [°]			
Phase	83.84 [°]	Phase	125.65 [°]			
22 Jan - 22 Mar 2015						
M2		M4			Residual current	
SEMA	0.611 [m/s]	SEMA	0.046 [m/s]	x		-0.007 [m/s]
SEMI	0.024 [m/s]	SEMI	0.02 [m/s]	y		-0.004 [m/s]
Inclination	68.2 [°]	Inclination	71.11 [°]			
Phase	83.21 [°]	Phase	129.42 [°]			
Difference						
M2		M4			Residual current	
SEMA	-0.005 [m/s]	SEMA	0.003 [m/s]	x		0.000 [m/s]
SEMI	0.001 [m/s]	SEMI	0.000 [m/s]	y		0.002 [m/s]
Inclination	-0.11 [°]	Inclination	0.08 [°]			
Phase	-0.63 [°]	Phase	3.77 [°]			

9.3 Scatter plots of x- and y- velocities

The correlation between the computed tidal ellipse and the gathered raw data is given in Fig. 21 and Fig. XX with R-squared values $R^2_x=0,82$ and $R^2_y=0,85$ for the x- and y-direction respectively.

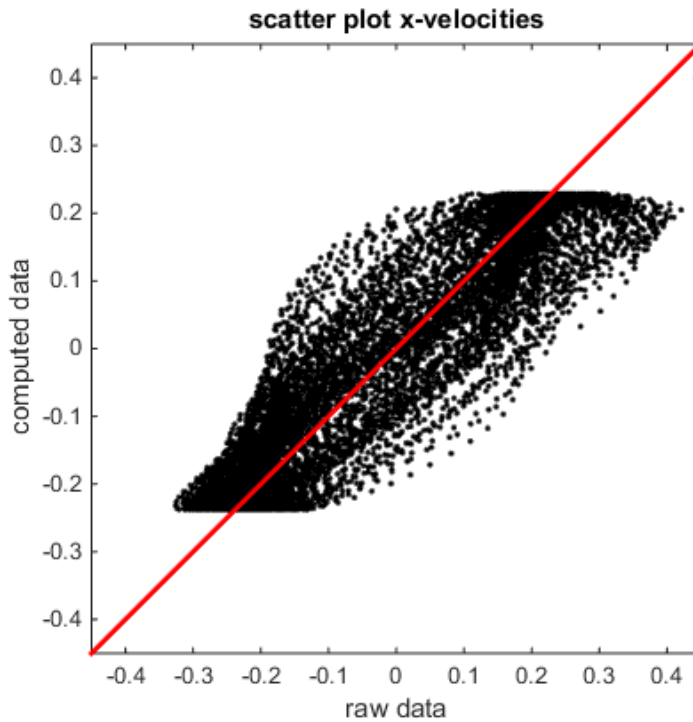


Figure 39 Scatter plot for x-velocities of computed tidal ellipse data versus the gathered raw data in MATROOS

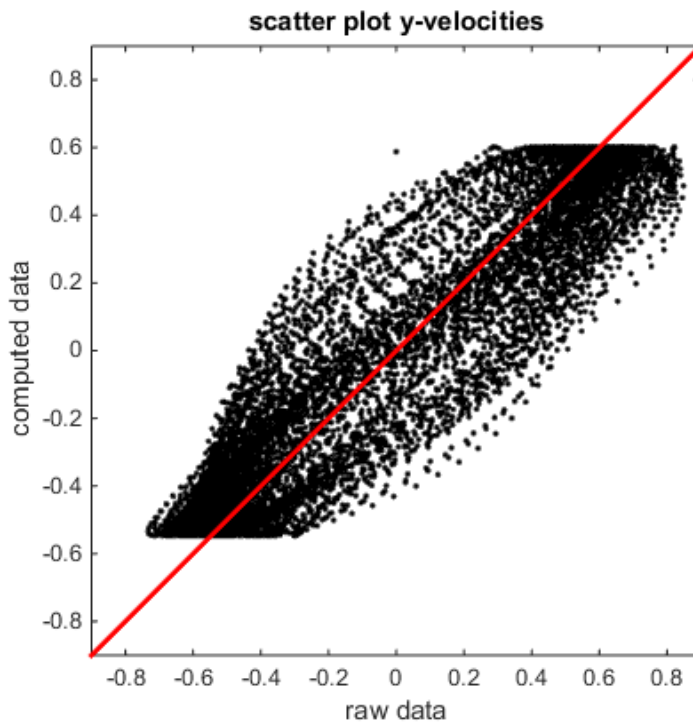


Figure 40 Scatter plot for y-velocities of computed tidal ellipse data versus the gathered raw data in MATROOS

9.4 Dike ring area 14

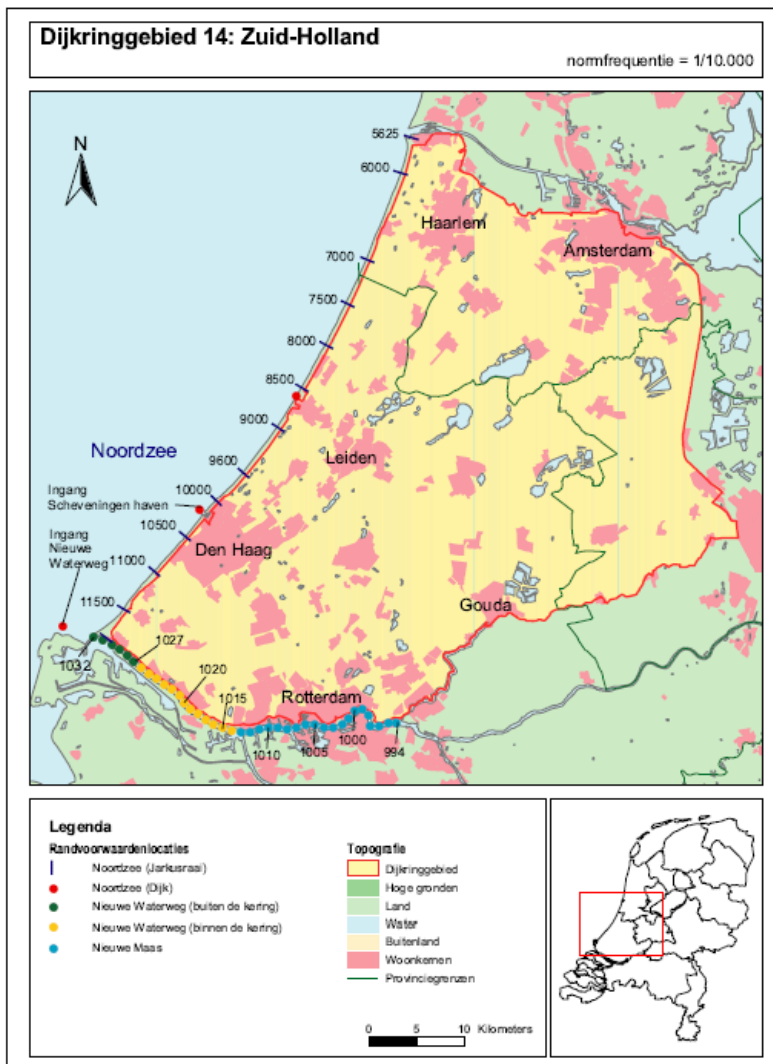


Figure 41 Overview of dike ring area 14 (Ministerie van Verkeer en Waterstaat, 2007).

The corresponding hydraulic boundary conditions are:

Table 13 Hydraulic boundary conditions per ray for dike ring 14 with exceedance probability of 1/10.000. For the rays see the overview map of dike ring 14. The "Rekenpeil" is the value used for the water level in the 1/10.000 event, the H_{m0} is the significant wave height and the T_p is the peak period of the wave (Ministerie van Verkeer en Waterstaat, 2007)

Omschrijving	Rekenpeil [m+NAP]	H_{m0} [m]	T_p [s]
Jarkus raai: van - tot			
5625-5800	5,7	9,25	16,0
5800-6400	5,7	9,15	15,8
6400-7150	5,8	9,00	15,5
7150-8000	5,8	8,85	15,0
8000-9750	5,8	8,55	14,3
9750-9900	5,8	8,35	13,9
9900-10140	5,7	8,30	13,8
10140-10996	5,7	8,05	13,2
11012-11700	5,7	7,90	12,8
11700-11850	5,6	7,70	12,3

9.5 Scaling procedure

Following the so-called *quasi-stationary* approach, two time-scales are distinguished: one associated with the hydrodynamics and one associated with the bed evolution. A ‘fast’ hydrodynamic time coordinate t and a ‘slow’ morphological time coordinate t_m are introduced

$$\begin{cases} t = \sigma^* t^* \\ t_m = \frac{t^*}{T_m^*} \end{cases} \text{ with } T_m^* = \frac{(1-\epsilon_p)H^*}{\sigma^* \alpha^* U^{*b-1}} \quad (9)$$

here T_m^* is in the order of several decades and in which H^* and U^* are used to scale the depth and velocity respectively, the derivation of the morphological time scale is given in chapter 9.5.1. It can be concluded from $\frac{t_m}{t} = (\sigma^* T_m^*)^{-1} \ll 1$ that the time scales are far apart. This indicates that bed changes within a tidal cycle can be neglected and only the tidally averaged sediment transport effectively contributes to the bed evolution (quasi-stationary approach).

The following dimensionless quantities are introduced

$$\mathbf{u} = \frac{\mathbf{u}^*}{U^*}, \quad \zeta = \frac{\zeta^*}{Z^*}, \quad h = \frac{h^*}{H^*}, \quad l_{mor}^* = \frac{U^*}{\sigma^*}, \quad \mathbf{x} = \frac{\mathbf{x}^*}{l_{mor}^*}, \quad (10)$$

where U^* and Z^* are used to scale the velocity and the free surface elevation. It follows that

$$u^*(x^*, y^*, t^*) = U^* u(x, y, t) = U^* u\left(\frac{x^*}{l_{mor}^*}, \frac{y^*}{l_{mor}^*}, \sigma^* t^*\right),$$

$$\text{so that, e.g., } \frac{\partial u^*}{\partial t^*} = U^* \frac{\partial u}{\partial t} \frac{\partial t}{\partial t^*} = U^* \sigma^* \frac{\partial u}{\partial t}.$$

This leads, after division of Eq. (2) by $U^* \sigma^*$, to the following scaled momentum equation in the x-direction:

$$\frac{\partial u}{\partial t} + u \frac{\partial u}{\partial x} + v \frac{\partial u}{\partial y} - \frac{f^*}{\sigma^*} v + \frac{r^*}{\sigma^* H_0^*} \frac{u}{h} = -g^* \frac{Z^*}{U^{*2}} \frac{\partial \zeta}{\partial x}. \quad (11)$$

Hence, new dimensionless quantities are introduced:

$$f = \frac{f^*}{\sigma^*}, \quad r = \frac{r^*}{\sigma^* H^*} \quad (12)$$

and since the term $g^* \frac{Z^*}{U^{*2}}$ in front of $\frac{\partial \zeta}{\partial x}$ is desired to be 1, it follows that $Z^* = \frac{U^{*2}}{g^*}$.

Hence, the scaled version of the momentum equation in x- Eq. (2) and y-direction Eq. (3) are given by

$$\frac{\partial u}{\partial t} + u \frac{\partial u}{\partial x} + v \frac{\partial u}{\partial y} - f v + r \frac{u}{h} = -\frac{\partial \zeta}{\partial x}, \quad (13)$$

$$\frac{\partial v}{\partial t} + u \frac{\partial v}{\partial x} + v \frac{\partial v}{\partial y} + f u + r \frac{v}{h} = -\frac{\partial \zeta}{\partial y}, \quad (14)$$

Filling in the dimensionless quantities in the conservation of mass equation results in

$$Z^* \sigma^* \frac{\partial \zeta}{\partial t} + \frac{U^*}{l_{mor}^*} \left(\frac{\partial}{\partial x} (h^* H^* + \zeta Z^*) u \right) + \frac{\partial}{\partial y} ((h^* H^* + \zeta Z^*) v^*) = 0. \quad (15)$$

Now the whole equation is divided by H^* and $\frac{U^*}{l_{mor}^*}$, so that

$$\frac{Z^* \sigma^* l_{mor}^*}{H^* U^*} \frac{\partial \zeta}{\partial t} + \left(\frac{\partial}{\partial x} \left(h + \zeta \frac{Z^*}{H^*} \right) u \right) + \frac{\partial}{\partial y} \left(\left(h + \zeta \frac{Z^*}{H^*} \right) v \right) = 0. \quad (16)$$

Since $Z^* = \frac{U^{*2}}{g^*}$, $\frac{Z^*}{H^*} = \frac{U^{*2}}{g^* H^*}$, which is the squared Froude number (Fr^2) and the value of the squared Froude number is very small $Fr^2 = \frac{U^{*2}}{g^* H^*} = 0.005$, with typical values

$U^* = 1 \text{ m/s}$, $g^* = 9.81 \text{ m/s}^2$, $H^* = 20 \text{ m}$ and $l_{mor}^* = \frac{U^*}{\sigma^*}$ this means that we can take the ($Fr^2 = 0$) limit of Eq. (15)

$$\frac{\partial}{\partial x} (hu) + \frac{\partial}{\partial y} (hv) = 0. \quad (17)$$

9.5.1 Sediment transport

The sediment transport equation in terms of the dimensionless quantities can be written as

$$\vec{q}^* = \alpha^* U^{*b} |\vec{u}|^b \left(\frac{\vec{u}}{|\vec{u}|} + \frac{\lambda^* H^*}{l_{mor}^*} \nabla h \right). \quad (18)$$

Hence new dimensionless quantities are introduced:

$$\vec{q} = \frac{\vec{q}^*}{\alpha^* U^{*b}}, \quad \lambda = \frac{\lambda^* H^*}{l_{mor}^*}, \quad (19)$$

so the equation becomes:

$$\vec{q} = |\vec{u}|^b \left(\frac{\vec{u}}{|\vec{u}|} + \lambda \nabla h \right). \quad (20)$$

9.5.1 Bed evolution

The bed evolution equation (7) in terms of the dimensionless quantities can be written as

$$\frac{H^*}{T_{mor}^*} \frac{\partial h}{\partial t_{mor}} = \frac{\alpha^* U^{*b}}{1-\epsilon_p} \frac{1}{l_{mor}^*} \left(\frac{\partial q_x}{\partial x} + \frac{\partial q_y}{\partial y} \right), \quad (21)$$

dividing the whole equation with $\frac{H^*}{T_{mor}^*}$ results in

$$\frac{\partial h}{\partial t_{mor}} = \frac{\alpha^* U^{*b} T_{mor}^*}{(1-\epsilon_p) H^* l_{mor}^*} \left(\frac{\partial q_x}{\partial x} + \frac{\partial q_y}{\partial y} \right). \quad (22)$$

The term $\frac{\alpha^* U^{*b} T_{mor}^*}{(1-\epsilon_p) H^* l_{mor}^*}$ in front of $\left(\frac{\partial q_x}{\partial x} + \frac{\partial q_y}{\partial y} \right)$ is desired to be 1, so it follows that

$$T_{mor}^* = \frac{(1-\epsilon_p) H^* l_{mor}^*}{\alpha^* U^{*b}}, \text{ where } l_{mor}^* = \frac{U^*}{\sigma^*}, \text{ so that}$$

$$T_{mor}^* = \frac{(1-\epsilon_p) H^*}{\alpha^* U^{*b-1} \sigma^*}. \quad (23)$$

Hence, the scaled bed evolution equation can now be written as

$$\frac{\partial h}{\partial t_{mor}} = \frac{\partial q_x}{\partial x} + \frac{\partial q_y}{\partial y}. \quad (24)$$

9.6 Solution method

As stated before, the pit depth is considered small compared to the water depth. This small perturbation allows for linearization w.r.t. the small parameter

$$\epsilon = \frac{H_{pit}^*}{H^*}. \quad (25)$$

Introducing a perturbed state $(h_1, \mathbf{u}_1, \zeta_1, \mathbf{q}_1)$, we write

$$\begin{pmatrix} h \\ \mathbf{u} \\ \zeta \\ \mathbf{q} \end{pmatrix} = \begin{pmatrix} 1 \\ u_0 \\ \zeta_0 \\ q_0 \end{pmatrix} + \epsilon \begin{pmatrix} h_1 \\ \mathbf{u}_1 \\ \zeta_1 \\ \mathbf{q}_1 \end{pmatrix}. \quad (26)$$

Linearizing works by filling in above terms in the equations for the basic state, taking the derivative to ϵ and then substituting $\epsilon = 0$. The model equations after linearizing are given in appendix 9.7.

To solve for the perturbed flow, the next step is to expand in a discrete Fourier series, according to

$$\begin{pmatrix} h_1 \\ \mathbf{u}_1 \\ \zeta_1 \end{pmatrix} = \sum_{m,n} \begin{pmatrix} 1 \\ \mathbf{U}_{mn}(t) \\ Z_{mn}(t) \end{pmatrix} H_{mn}(t_m) \exp(i\mathbf{k}_{mn} \mathbf{x}). \quad (27)$$

The model now considers the pit as a summation of individual modes, with complex bed amplitude H_{mn} , where m and n range from $-M$ to M and from $-N$ to N , respectively. We choose $M = N = 128$, with real and imaginary parts in both x- and y-direction, so $(128^2)^2 = 65536$ individual signals. Furthermore, U_{mn} and Z_{mn} are the time-dependent Fourier components of the perturbed flow and perturbed surface elevation, respectively. Finally, $\mathbf{k}_{mn} = (k_m, l_n)$ is the topographic wave vector of the (m, n) -th mode, containing wave numbers in both horizontal directions:

$$k_m = k_{min} m, \quad l_n = k_{min} n, \quad (28)$$

here $k_{min} = \frac{2\pi L_{mor}^*}{L_{dom}}$ is the minimum wave number.

For each Fourier component the perturbed state is calculated, in which the perturbed flow induces sediment transport. As a direct result of the linear approach, the bed amplitudes of the individual modes satisfy a linear differential equation

$$\frac{\partial H_{mn}}{\partial t_m} = \omega_{mn} H_{mn}, \quad H_{mn}(0) = H_{mn}^{init}, \quad (29)$$

so that the solution displays exponential growth or decay:

$$H_{mn}(t_m) = H_{mn}^{init} \exp(\omega_{mn} t_m), \quad (30)$$

here H_{mn}^{init} corresponds to the initial amplitude of the individual signal and ω_{mn} is the growth rate per signal. This complex quantity reflects all the morphodynamic, where the real part

represents the growth or decay and the imaginary part is associated with the migration rate given by

$$c_{mig} = -\frac{\omega_i}{\sqrt{k_x^2 + k_y^2}}. \quad (31)$$

This calculation is done for each individual signal and with all these new signals the eventual bathymetry for an arbitrary point in time can be calculated with an inverse Fourier transformation.

9.7 Linearizing the equations with respect to the bed amplitude.

To linearize the scaled equations of the 2015 sand pit model, the dimensionless parameter $\epsilon = \frac{H_{pit}^*}{H^*}$ is used (Eq. 25). We fill in the approximations of Eq. 26 in the scaled equations, and take the derivative to ϵ and then substitute $\epsilon = 0$. The linearization of the momentum equation in the x-direction (Eq. 13) is as follows:

$$\frac{\partial(u_0 + \epsilon u_1)}{\partial t} + (u_0 + \epsilon u_1) \frac{\partial(u_0 + \epsilon u_1)}{\partial x} + (v_0 + \epsilon v_1) \frac{\partial(u_0 + \epsilon u_1)}{\partial y} - f(v_0 + \epsilon v_1) + r \frac{(u_0 + \epsilon u_1)}{(h_0 + \epsilon h_1)} = -\frac{\partial(\zeta_0 + \epsilon \zeta_1)}{\partial x}, \quad (32)$$

now the derivative to ϵ is taken and we then substitute $\epsilon = 0$. How each term of Eq. (32) is linearized is presented below:

First term:

$$\frac{\partial(u_0 + \epsilon u_1)}{\partial t} \xrightarrow{\frac{\partial}{\partial \epsilon}} \frac{\partial u_1}{\partial t}. \quad (33)$$

Second term:

$$(u_0 + \epsilon u_1) \frac{\partial(u_0 + \epsilon u_1)}{\partial x} \rightarrow u_0 \frac{\partial u_0}{\partial x} + \epsilon \left(u_0 \frac{\partial u_1}{\partial x} + u_1 \frac{\partial u_0}{\partial x} \right) + \epsilon^2 u_1 \frac{\partial u_1}{\partial x} \xrightarrow{\frac{\partial}{\partial \epsilon}} \left(u_0 \frac{\partial u_1}{\partial x} + u_1 \frac{\partial u_0}{\partial x} \right) + 2\epsilon u_1 \frac{\partial u_1}{\partial x} \xrightarrow{\epsilon=0} \left(u_0 \frac{\partial u_1}{\partial x} + u_1 \frac{\partial u_0}{\partial x} \right), \quad (34)$$

but $\frac{\partial u_0}{\partial x} = 0$ because of the spatial uniformity in the reference situation, so we end up with

$$u_0 \frac{\partial u_1}{\partial x}. \quad (35)$$

Third term, similar to the second term:

$$(v_0 + \epsilon v_1) \frac{\partial(u_0 + \epsilon u_1)}{\partial y} \xrightarrow{\frac{\partial}{\partial \epsilon} |_{\epsilon=0}} v_0 \frac{\partial u_1}{\partial y}. \quad (36)$$

Fourth term:

$$-f(v_0 + \epsilon v_1) \xrightarrow{\frac{\partial}{\partial \epsilon}} -f v_1. \quad (37)$$

Fifth term:

$$r \frac{(u_0 + \epsilon u_1)}{(1 + \epsilon h_1)} \xrightarrow{\frac{\partial}{\partial \epsilon}} r \frac{u_1(1 + \epsilon h_1) - (u_0 + \epsilon u_1)h_1}{(1 + \epsilon h_1)^2} \xrightarrow{\epsilon=0} ru_1 - ru_0 h_1. \quad (38)$$

Sixth term:

$$-\frac{\partial(\zeta_0 + \epsilon \zeta_1)}{\partial x} \xrightarrow{\frac{\partial}{\partial \epsilon}} -\frac{\partial \zeta_1}{\partial x}. \quad (39)$$

so the linearized momentum equation in the x-direction becomes:

$$\frac{\partial u_1}{\partial t} + u_0 \frac{\partial u_1}{\partial x} + v_0 \frac{\partial u_1}{\partial y} - f v_1 + ru_1 - ru_0 h_1 = -\frac{\partial \zeta_1}{\partial x}. \quad (40)$$

Likewise for the equations of the momentum equation in the y-direction (Eq. 14), so that the linearized equation reads

$$\frac{\partial v_1}{\partial t} + u_0 \frac{\partial v_1}{\partial x} + v_0 \frac{\partial v_1}{\partial y} + f u_1 + r v_1 - r v_0 h_1 = -\frac{\partial \zeta_1}{\partial y}. \quad (41)$$

The linearized version of the conservation of mass (Eq. 16) reads

$$\frac{\partial u_1}{\partial x} + \frac{\partial v_1}{\partial y} = -u_0 \frac{\partial h_1}{\partial x} - v_0 \frac{\partial h_1}{\partial y}. \quad (42)$$

The linearized version of the sediment transport (Eq. 20) reads

$$\mathbf{q}_1 = (b-1)|\bar{\mathbf{u}}_0|^{b-3}(\bar{\mathbf{u}}_0 \cdot \bar{\mathbf{u}}_1)\bar{\mathbf{u}}_0 + |\bar{\mathbf{u}}_0|^{b-1}\bar{\mathbf{u}}_1 + \lambda|\bar{\mathbf{u}}_0|^b \vec{\nabla} h_1, \quad (43)$$

with the two-dimensional nabla-operator $\vec{\nabla} = (\frac{\delta}{\delta x}, \frac{\delta}{\delta y})$.

Finally, the linearized version of the bed evolution (Eq. 24) reads

$$\frac{\partial h_1}{\partial t_m} = \frac{\partial q_{1,x}}{\partial x} + \frac{\partial q_{1,y}}{\partial y}. \quad (44)$$